Paleoceanography and Paleoclimatology

AGU ADVANCING EARTH AND SPACE SCIENCE

RESEARCH ARTICLE
10.1029/2021PA004236

Special Section:
Cenozoic Evolution of Mountains, Monsoons, and the Biosphere

Palaeoceanography of the Japan Sea Across the Mid-Pleistocene Transition: Insights From IODP Exp. 346, Site U1427

Sonja Felder[1], Takuya Sagawa[2], Mervyn Greaves[3], Melanie J. Leng[4,5], Ken Ikehara[6], Katsunori Kimoto[7], Siro Hasegawa[8], Thomas Wagner[9], and Andrew C. G. Henderson[1]

[1]School of Geography, Sociology and Politics, Newcastle University, Newcastle Upon Tyne, UK, [2]Institute of Science and Engineering, Kanazawa University, Kanazawa, Japan, [3]Department of Earth Sciences, University of Cambridge, Cambridge, UK, [4]National Environmental Isotope Facility, British Geological Survey, Nottingham, UK, [5]School of Biosciences, Nottingham University, Nottingham, UK, [6]Geological Survey of Japan, National Institute of Advanced Industrial Science and Technology (AIST), Tsukuba, Japan, [7]Japan Agency for Marine-Earth Science and Technology (JAMSTEC), Yokosuka, Japan, [8]The Tohoku University Museum, Sendai, Japan, [9]The Lyell Centre, School of Energy Geoscience Infrastructure and Society, Heriot-Watt University, Edinburgh, UK

Key Points:

- A high-resolution, continuous benthic foraminiferal oxygen isotope record is presented using sediments of IODP Site U1427 (Exp. 346)
- MIS 24-17 are characterized by the glacial near isolation of the Japan Sea, while for stages 39-25 an improved connection is suggested
- Presenting a new core-top Mg/Ca-temperature calibration for *Uvigerina spp*. from the Japan Sea and revised age model for IODP Site U1427

Supporting Information:

Supporting Information may be found in the online version of this article.

Correspondence to:

S. Felder,
s.felder1@ncl.ac.uk;
sonja.felder@ewetel.net

Citation:

Felder, S., Sagawa, T., Greaves, M., Leng, M. J., Ikehara, K., Kimoto, K., et al. (2022). Palaeoceanography of the Japan sea across the mid-Pleistocene transition: Insights from IODP exp. 346, site U1427. *Paleoceanography and Paleoclimatology*, *37*, e2021PA004236. https://doi.org/10.1029/2021PA004236

Received 4 FEB 2021
Accepted 9 NOV 2021

Author Contributions:

Formal analysis: Thomas Wagner
Resources: Thomas Wagner
Supervision: Thomas Wagner

Abstract Large-scale atmospheric circulation patterns, such as the East Asian monsoon, have been proposed as possible feedbacks of the mid-Pleistocene transition (MPT). Marine sediments of the Japan Sea (JS) record variations in the East Asian monsoon over long timescales and may be crucial for understanding of the MPT. To interpret these sediments correctly an understanding of the JS palaeoceanography is necessary. So far, the JS palaeoceanography has been extrapolated across the MPT from studies of the most recent glacial-interglacial cycles. These suggest a good connection and unrestricted water-mass exchange with the open ocean during interglacial sea-level highstands, while during glacial sea-level lowstands the JS is nearly isolated. Glacial isolation often results in poor carbonate preservation and unusually low oxygen isotope ($\delta^{18}O$) ratios from low-saline/low-$\delta^{18}O$ waters accumulating in the basin. Using the sediments of Integrated Ocean Drilling Program (IODP) Site U1427, a shallow-water site in the southern JS, we present a continuous foraminiferal $\delta^{18}O$ record encompassing the MPT. This record shows the JS-typical low glacial $\delta^{18}O$ values in the late phase of the MPT, across Marine Isotope Stages (MIS) 24-17, while earlier MPT glacials, across MIS 39-25, are characterized by high $\delta^{18}O$ values. We propose that high glacial $\delta^{18}O$ values are the result of an improved connection between the shallow, southern JS and adjacent ocean during early MPT glacials. The impact of this palaeoceanographic mode, if continued to deep-water sites, would make the interpretation of dark/light sediment layers as glacial/interglacial deposits uncertain.

1. Introduction

1.1. The Mid-Pleistocene Transition and the East Asian Monsoon

The Quaternary period is characterized by glacial-interglacial variability that has been linked to Earth's orbital cyclicity (e.g., Hays et al., 1976; Ruddiman, 2001). During the early part of the Quaternary, glacial-interglacial cycles varied at a frequency of 41,000 years (41 ka), but approximately half-way through the Quaternary, during the mid-Pleistocene, the glacial-interglacial cyclicity shifted to quasi 100,000 years (100 ka) cycles (e.g., Lisiecki & Raymo, 2005; Zachos et al., 2001). The transition period between 41 ka and 100 ka is centred at ~1200 to 600 ka and often referred to as the mid-Pleistocene transition (MPT). After the MPT, glacials became more intense, producing larger ice-sheets that decayed more rapidly at glacial terminations (e.g., Lisiecki & Raymo, 2005; Pisias & Moore, 1981; Shackleton & Opdyke, 1976) and greater sea-level variations, as inferred from global, open ocean sea-level reconstructions (e.g., Bintanja et al., 2005; Berends et al., 2019; Elderfield et al., 2012; Rohling et al., 2014). Before the MPT (~2,700–1200 ka), global eustatic sea-level fluctuations were small, having an average glacial sea-level drop of ~–60 to −80 m, compared to the larger sea-level falls of the last ~900 ka, when glacial sea-levels were up to 120m ± 32 m lower than at present (*c.f.* Sosdian & Rosenthal, 2009). Crucially, the MPT occurred in the absence of changes in orbital/Milankovitch forcing, implying the mechanisms for the emergence of the 100 ka cycles are internal to the Earth's climate system. Proposed forcing mechanisms include changes in ice-sheet dynamics (e.g., Chalk et al., 2017; Clark et al., 2006; Imbrie et al., 1993; Raymo

et al., 1997) and feedback mechanisms associated with changes in the carbon cycle, including atmospheric CO_2 drawdown and ocean carbon storage (e.g., Chalk et al., 2017; DeMenocal, 1995; Farmer, Goldstein, et al., 2019; Hönisch et al., 2009; Higgins et al., 2015; Hasenfratz et al., 2019; Kender et al., 2018; Lear et al., 2016; Martínez-Garcia et al., 2011; Pena & Goldstein, 2014; Ruddiman, 2003, 2004; Sosdian et al., 2018; Shackleton, 2000). Large-scale atmospheric circulation patterns, such as the East Asian monsoon, have also been suggested as possible important influences, acting as fast conveyers of climate signals and triggers between ocean basins and across continents (Clark et al., 1999; Kubota et al., 2010; Porter & An, 1995; Tada, 2004; Tada et al., 2015a).

Records of past East Asian monsoon variations, particularly of the East Asian summer monsoon, which is characterized by its precipitation, can be found in continental archives, such as speleothems of Chinese caves, and lake and/or loess-paleosol sequences on the Chinese Loess Plateau (Cheng et al., 2016; Ruddiman, 2001; Wang et al., 2001; Wang et al., 2008). These are, however, not ideal archives to trace the monsoon across the MPT, for example, as they do not encompass the MPT (longest Chinese speleothem record ∼640 ka, longest lake record ∼20 ka), can contain gaps/hiatuses (e.g., lakes that do not record when dried out, erosion of loess deposits), and there is debate about whether they record the monsoon precipitation intensity or rather atmospheric circulation changes (Cheng et al., 2016; Clemens et al., 2010; Lu et al., 2006; Maher & Thompson, 2012; Obreht et al., 2019; Wang et al., 2001; Wang et al., 2008; Zhang et al., 2018). Marine records of East Asian summer monsoon variations may be more reliable as they record regional precipitation changes through freshwater runoff and they may also be more complete (Clemens et al., 2018).

1.2. Influences of Variations in Glacio-Eustatic Sea-Level and the East Asian Summer Monsoon on Japan Sea Palaeoceanography

The Japan Sea (JS) palaeoceanography is sensitive to variations in glacio-eustatic sea-level due to its shallow sills connecting it with the open ocean, all being shallower than 130 m at present (Lee & Choi, 2015; Oba et al., 1991; Tada, 1994; Tada et al., 1999; Figure 1). The main inflow to the JS is the Tsushima Warm Current (TWC), which enters through the Tsushima Strait (TSS) in the south (Figure 1). It is estimated that during sea-level lowstands of the most recent glacials, around −134 to −120 m (Lambeck et al., 2014; Sosdian & Rosenthal, 2009), most of the TSS sill (present water depth ∼130 m) had dried up and there was negligible inflow (Matsui et al., 1998; Tada et al., 1999), leaving the JS nearly isolated (Ingle, 1975; Matsui et al., 1998; Oba et al., 1991; Saavedra-Pellitero et al., 2019; Tada, 1994; Tada et al., 1999; Watanabe et al., 2007).

In addition to the glacio-eustatic influences, the JS is also characterized by variations in the East Asian summer monsoon precipitation. Part of the monsoon precipitation from the East Asian hinterland enters through two of the world's largest rivers, the Yangtze and Yellow Rivers (e.g., Zhang et al., 2016), both of which drain onto the East China Sea shelf (Figure 1). Here the freshwater mixes with ocean waters, reducing sea-water salinities and increasing water nutrient contents, and forming the East China Sea Coastal Water (ECSCW). A branch of the ECSCW is directed into the JS, where it joins the Tsushima Warm Current (Figure 1), and its warm, nutrient-enriched waters prime marine productivity (e.g., Oba et al., 1991; Saavedra-Pellitero et al., 2019; Tada et al., 1999).

As a result of the (near) isolation of the JS and the input of low saline waters (ECSCW, precipitation over the basin, river runoff from surrounding landmasses) during glacials, the water column becomes stratified. This stratification can lead the bottom waters at >500 m water depth to become corrosive to carbonates, resulting in widespread carbonate dissolution (e.g., Dunbar et al., 1992; Ikehara, 1991; Ikehara et al., 1994; Kido et al., 2007; Oba et al., 1991; Tada, 1994; Tada et al., 1992).

The poor carbonate preservation causes incomplete microfossil and foraminifera-based oxygen isotope records, $\delta^{18}O$, resulting in difficulties and hindering the establishment of robust geochronologies for JS sediments (Dunbar et al., 1992; Oba et al., 1991; Tada, 1994). Furthermore, the accumulation of low-saline and, more crucially, low-$\delta^{18}O$ waters can imprint on $\delta^{18}O$ records, leading to unusually low glacial $\delta^{18}O$ values and making records challenging and often counterintuitive to interpret (Oba et al., 1991; Saavedra-Pellitero et al., 2019; Sagawa et al., 2018; Tada, 1994; Tada et al., 1992; Tada et al., 1999). During the Last Glacial maximum, for example, the input of large amounts of monsoon runoff/freshwater evened out glacial temperature drops in foraminiferal $\delta^{18}O$ records of the JS (Oba et al., 1991; Oba & Irino, 2012).

Detailed studies of the connection between the JS palaeoceanography and variations in monsoon precipitation, i.e., relative contributions of ECSCW to the TWC, exist for the sediments of ODP Site 797 (∼2,860 m water

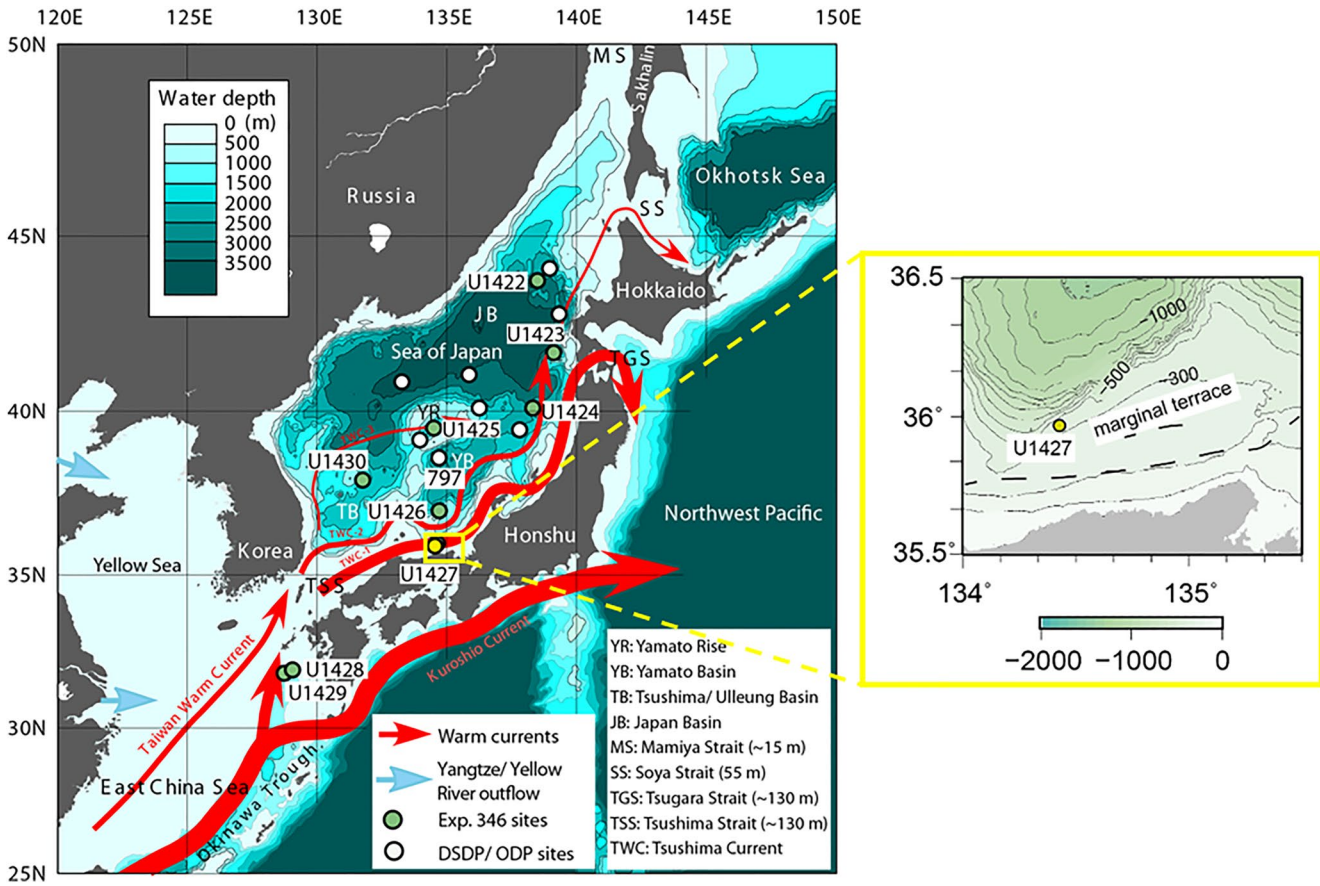

Figure 1. Bathymetric map of the Japan Sea illustrating locations of DSDP/ODP/IODP sites, including IODP/ODP Sites U1427 (yellow) and 797 (north of Site U1427 in the Yamato Basin) (modified from Tada et al., 2013), and major ocean current systems, including the branches of the Tsushima Warm Current (TWC) in the Japan Sea (red arrows, after Inoue, 1989, and Tomczak & Godfrey, 1994) and the approximate position of Yellow and Yangtze River mouths in the Yellow and East China Seas (blue arrows). Sill depths, including the Tsushima Strait (TSS) in the south, are given in the legend (after Lee & Choi, 2015; Oba et al., 1991; Tada et al., 1999). The insert is showing an enlarged bathymetric map, depicting the marginal terrace on which Site U1427 is located (modified from Sagawa et al., 2015) with approximate positions of major tectonic fault zones (dashed lines, after Itoh et al., 2002).

depth; Tada et al., 1999) and the upper 250 m of IODP Site U1427 (~330 m water depth; Saavedra-Pellitero et al., 2019; both sites in Figure 1). Tada et al. (1999) analyzed metre to sub-metre scale sediment color alternations–dark (interstadial) and light (stadial) – at ODP Site 797, encompassing the last ~200 ka (MIS 1-7). It is suggested that at sea-level stands greater than ~90 m below present (TSS sill water depth <40 m), the JS was isolated from the open ocean and the excess of precipitation over evaporation resulted in a stratified water column and low marine productivity (Tada et al., 1999). At sea-level stands of −90 to −60 m (TSS sill depth 40 to 70 m), the JS was semi-isolated, i.e., not isolated enough to form a persistent low-salinity surface layer and with slightly enhanced marine productivity. Instead, water mass stratification varies with ECSCW contributions to the TWC, as a consequence of variations in the East Asian summer monsoon (Tada et al., 1999). At intermediate sea-levels of −60 to −20 m (TSS sill 70 to 100 m), inflow via the TSS is significant, and marine productivity, deep water oxygenation/water mass stratification and organic matter preservation vary with the monsoon, i.e., the ECSCW contribution to the TWC (Tada et al., 1999). For example, at times of enhanced monsoon precipitation the ECSCW contribution to the TWC is enhanced, leading to increased marine productivity and a stronger water mass stratification due to the low-saline, high-nutrient composition of ECSCW. In contrast, at times of weaker monsoon at intermediate sea-levels, the contribution of ECSCW to the TWC is reduced, leading to reduced marine productivity and likely a better mixed water column. The oscillations in marine productivity, associated with sea-level and ECSCW contribution at intermediate sea-levels (−90 to −20 m), have recently been corroborated by a coccolithophore assemblage study of a shallow water site in the JS, Site U1427 (Saavedra-Pellitero et al., 2019, Figure 1). At sea-levels of −20 to +10 m, inflow via the TSS is high and the relative contribution of ECSCW is

reduced, resulting in improved deep-water ventilation and high marine carbonate productivity (Saavedra-Pellitero et al., 2019; Tada et al., 1999).

This sensitivity of the JS palaeoceanography to glacio-eustatic sea-level variations suggests its sediments might have recorded the intensity increase in glacial-interglacial cycles and associated sea-level fluctuations that occurred across the MPT (e.g., Berends et al., 2019; Bintanja et al., 2005; Elderfield et al., 2012; Rohling et al., 2014). A detailed study of the JS palaeoceanography and its potential response to the increased fluctuations across the MPT has, however, not yet been carried out. In part, this information has not been generated because the MPT is often condensed into just ∼10 to 50 m of sediments at deep-water sites (see e.g., Expedition reports and associated studies for ODP Legs 127/128 by Ingle et al., 1990, or Tamaki et al., 1992, and for IODP Exp. 346 by Tada et al., 2013, 2015a) but it is also influenced by issues of dating JS sediments.

1.3. This Study

Recently recovered sediments from a shallow-water site in the southern JS, IODP Site U1427 (∼330 m water depth, Figure 1), have good carbonate preservation throughout the cored interval, including across the MPT (e.g., Tada et al., 2015b). Due to constant, high sedimentation rates, the sediments record the MPT in high resolution across approximately 250 m of sediment cores (Gallagher et al., 2018; Irino et al., 2018; Saavedra-Pellitero et al., 2019; Sagawa et al., 2018; Tada et al., 2015b).

The palaeo-water depth across the MPT is difficult to estimate. On the one hand, removing the sediment column deposited since the MPT and compensating for porosity/compaction implies that palaeo-water depth could have been much greater than at present. On the other hand, while this approach may be applicable to passive margin settings, the tectonics in the JS, including Site U1427, are more complex. It has been shown that in the southwestern JS, near U1427, relatively complex tectonic activities are taking place (e.g., Itoh et al., 2002; Ismail-Zadeh et al., 2013; Okuno et al., 2014), and the overall structure, with horst and graben features that form the marginal terrace on which U1427 is located (Figure 1), are the result of extensional tectonics in a back-arc basin. Therefore, the vertical tectonic movement of the site was more likely one of subsidence, although there is recent strike-slip reactivation of the faults (*op. cit.*). While high resolution tectonic reconstructions for the MPT are not available, a general assumption of a net subsidence of the Site U1427 location would mean that the downward tectonic movement counteracted sediment accumulation. Lithological features, such as the absence of dark/light sediment lamination, also indicate that the sediments encompassing the MPT at Site U1427 remained at shallow water depths of less than 500 m (Ikehara et al., 1994; Oba et al., 1991; Tada et al., 1999; Tada et al., 2018).

Recent studies on the sediments enabled the production of a high-resolution, benthic foraminifera-based $\delta^{18}O$ record, encompassing the last ∼850 ka (MIS 1-21; Figure S4a in Supporting Information S1; Sagawa et al., 2018). This record shows relatively lower $\delta^{18}O$ values during glacials (when resolved), while interglacials are characterized by higher $\delta^{18}O$ values (Sagawa et al., 2018). While much work has been done on the upper 250 m of sediment cores, little work has yet been done on the sediments that encompass the MPT (Black et al., 2018; Gallagher et al., 2018; Miller & Dickens, 2017; Peterson & Schimmenti, 2020; Saavedra-Pellitero et al., 2019; Sagawa et al., 2018). The aim of this study is therefore twofold. First, we generate an orbital-scale geochronology for the JS encompassing the MPT, based on a foraminiferal $\delta^{18}O$ record from Site U1427 sediment cores. Using this age model, we examine the palaeoceanographic changes that have occurred in response to increasing amplitudes of glacial sea-level fluctuations. This information can be used to disentangle eustatic sea-level from monsoon signals and pave the way for detailed studies of the East Asian summer monsoon history on these sediments, to investigate its potential role during the MPT.

The foraminiferal $\delta^{18}O$ record presented in this study is affected by global ice volume/sea-level changes, as well as salinity influences and possibly sea-level-induced temperature changes given its shallow setting and likely tectonic history (see above). Therefore, low glacial $\delta^{18}O$ values could be induced by a sea-level drop (for example, from 330 m water depth at present to between −134 to −120 m, similar to the last glacial maximum; Lambeck et al., 2014; Sosdian & Rosenthal, 2009; Tada et al., 2015b), resulting in a shallower water depth and possibly a relative increase in bottom water temperatures. In contrast, interglacials place the site at greater water depths and likely lower bottom water temperatures, which would increase $\delta^{18}O$ values. It may therefore be difficult to decipher glacials from interglacials based on $\delta^{18}O$-based temperature estimates only.

To disentangle the local freshwater from the global ice volume/temperature signal in the JS $\delta^{18}O$ records, an additional proxy for either temperature or salinity is needed, such as Mg/Ca ratios (e.g., Elderfield et al., 2012; Elderfield & Ganssen, 2000; Nürnberg, 1995; Raymo et al., 2018; Rosenthal, 2007; Rosenthal et al., 1997; Sosdian & Rosenthal, 2009). Potential effects of environmental variables other than temperature on the Mg/Ca ratio of even diagenetically unaffected, well-preserved benthic foraminifera like the ones used here (such as morphotypes, regional differences, water carbonate saturation) are possible. However, *Uvigerina*-based core top calibrations have proven Mg/Ca ratios to be one of the most robust palaeo-temperature proxies available, especially if a region-specific calibration is applied (e.g., Stirpe et al., 2021, and references therein). Furthermore, the combination of Mg/Ca and $\delta^{18}O$ of foraminiferal carbonate records enables reconstructing the palaeo-seawater $\delta^{18}O$, which has not previously been shown for the JS (see Text S4 in Supporting Information S1).

2. Materials and Methods

2.1. Site U1427

IODP Site U1427, located in the southern JS in a shallow water depth of ~330 m, was drilled during IODP Expedition 346 ("Asian monsoon"), which gathered sediment cores from the JS and East China Sea (Tada et al., 2015a, 2015b). Sediments are light colored (olive gray to grayish green), homogenous/heavily bioturbated silty clays with intercalated ash layers and without light/dark color alternations present in the sediment of deeper-water JS sites, where they represent millennial-scale changes (Tada et al., 2015a, 2015b). Shipboard analyses show a correlation between the sediment color (documented by the reflectance index, b*) and the relative contributions of biogenic material and clays. Clays show a higher bulk sediment density and high values in the Natural Gamma Ray (NGR) log, a result of dense packing and higher contents of Potassium and Thorium, as well as low b* values, while biogenic material shows relatively lower density and NGR with higher b* values (Tada et al., 2015b). Variations in these data coincide with orbital cyclicity, as a result of the inflow of nutrient-rich waters via the TSS (Figure 1), where increased inflow during interglacials primes marine productivity, leading to high b* values, thus making the b* index a useful tool to help identify glacials and interglacials in the sediments. This approach was applied to the upper ~350 m of cored sediments, where it, combined with an *Uvigerina* spp.-based $\delta^{18}O$ record, enabled the identification of MIS 1-21 (Figure S4a in Supporting Information S1; Sagawa et al., 2018).

The depth scale applied in this study is "m U1427_Patched_CCSF-D(_rev20170310)" as shown in Irino et al. (2018), and as used by other publications on the upper ~250 m sediment cores of Site U1427 (Black et al., 2018; Gallagher et al., 2018; Miller & Dickens, 2017; Peterson & Schimmenti, 2020; Saavedra-Pellitero et al., 2019; Sagawa et al., 2018). The depth scale constructed by Irino et al. (2018) is applicable to the full splice interval, that is the upper 430.337 m CCSF-A, and for the non-splice interval below 11.755 m were added to CCSF-A depths to obtain the "Patched"-equivalent depth scale. This depths scale is referred to as "m CCSF-D_Patched" throughout this study.

2.2. Foraminiferal $\delta^{18}O$ Record

A benthic foraminiferal $\delta^{18}O$ record based on the genus *Uvigerina* spp. was generated, using the well-preserved shells of Site U1427 (Figure 2; see Text S2 in Supporting Information S1). Sediment samples were washed over a 63 µm mesh using deionized water (DI), dried at 50°C and dry-sieved on 150 µm mesh. Well-preserved *Uvigerina* spp. shells were isolated from the >150 µm fraction and cleaned using DI and agitation in an ultrasonic bath to remove contaminants. The rigor of the cleaning step was checked under a light microscope. For each analysis 50 to 100 µg of carbonate, corresponding to about 8 to 15 cleaned *Uvigerina* spp. shells, was measured using an IsoPrime dual inlet isotope ratio mass spectrometer plus multi-preparation device at the NERC Isotope Geosciences Laboratories (Keyworth, UK), alongside the in house reference material (KCM). 36 duplicate analyses showed relative standard deviations (r.s.d.) of ~0.08 ‰. All data is presented in the δ-notation against the Vienna Pee Dee belemnite (VPDB)-scale.

2.3. Foraminiferal Mg/Ca Ratios

Samples were selected from two intervals, 300–395 m and 460–525 m CCSF-D_Patched, to confirm the interpretation of the $\delta^{18}O$ record. For each analysis ~300 µg of uncleaned calcite was used, which approximated to about 10 to 30 *Uvigerina* spp. shells, all in good preservation state, i.e., showing little sign of diagenetic overgrowths

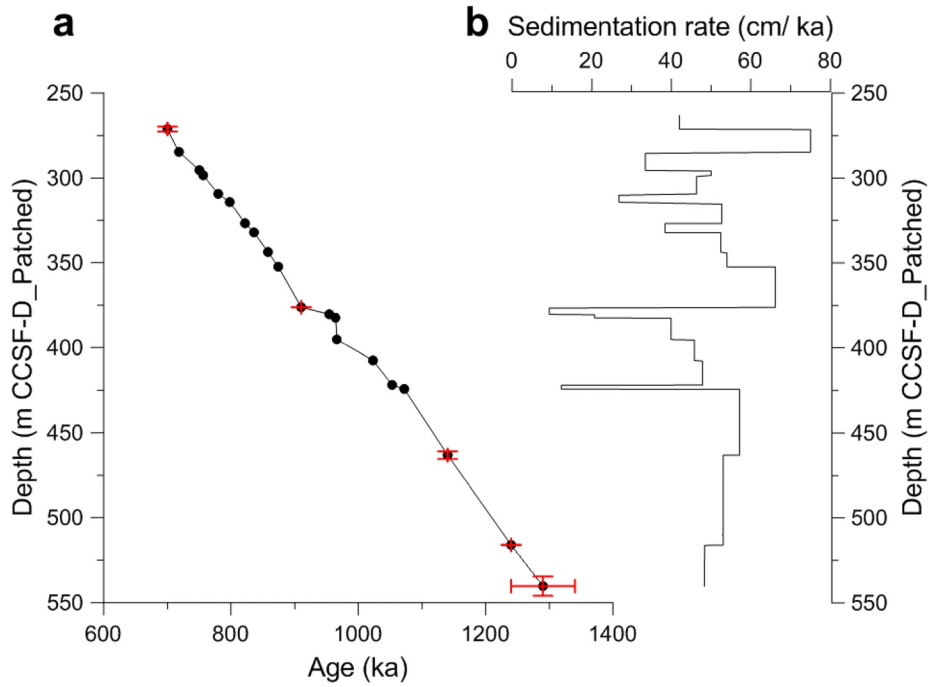

Figure 2. Age-depth relationship (Figure 2a) and calculated sedimentation rates (Figure 2b) encompassing ~250 to 550 m CCSF-D_Patched of Site U1427. Black dots in Figure 2a represent age tie points as listed in Table S1 (Supporting Information S1), with red bars indicating their respective uncertainties in depth and age where available (*c.f.* Tada et al., 2015b; Sagawa et al., 2018).

(see Text S2 in Supporting Information S1). The shells were cleaned using the Mg-/oxidative cleaning protocol after Barker et al. (2003) and analyzed on an Agilent inductively coupled plasma-optical emission spectrophotometer (ICP-OES) at the Godwin Laboratory for Palaeoclimate Research (Cambridge, UK), applying an intensity ratio calibration after De Villers et al. (2002). For quality control two reference solutions were analyzed, an in-house standard (Soln R3) and an international, external standard (JCt-1), which both show a precision (r.s.d.) of below 0.5%. The accuracy of Mg/Ca determinations has been established by interlaboratory studies (Greaves et al., 2008; Rosenthal et al., 2004) and was confirmed here by replicate analyses of standard JCt-1 where mean Mg/Ca of 1.266 mmol/mol (six replicates with standard deviation 0.005 and r.s.d. 0.40%) was obtained for JCt-1, in agreement with published results (Hathorne et al., 2013). A set of contaminant-indicating elements (Al, Ba, Fe, K, Mn, Na, Si, Ti, Zn) were determined simultaneously during each analytical run to monitor cleaning efficiency and diagenesis (*c.f.* Barker et al., 2003). Reproducibility between samples was tested on seven duplicates, split before cleaning, which show r.s.d. below 5%.

2.4. Temperature Estimates Based on Mg/Ca Ratios

A newly established Mg/Ca-temperature calibration based on *Uvigerina akitaensis* from the JS was used to calculate palaeo-water temperatures (Text S3 in Supporting Information S1). This new calibration extends the calibration range to lower temperatures, in a temperature range where few other calibrations for *Uvigerina* spp. are available (Elderfield et al., 2010; Roberts et al., 2016; Skinner et al., 2020). Besides being more comprehensive at low temperatures, this new calibration is based on the same genus (*Uvigerina*) and the same location (Japan Sea) and is hence being tuned to the regional setting of Site U1427, reducing local water mass effects (such as carbonate ion saturation, e.g., Elderfield et al., 2006; Martin et al., 2002) and increasing confidence in the calculated temperatures.

The newly established calibration is based on *Uvigerina akitaensis* from 16 core-top samples across a water depth-temperature transect at constant salinity in the JS (see, Text S3 and Figure S3 in Supporting Information S1) following the equation:

$$\text{Temperature } (^{\circ}\text{C}) = \left(\frac{\text{Mg}}{\text{Ca}} - 0.637\right) / 0.089$$

(see Text S3 in Supporting Information S1, Equation 2 is reprinted here for reference). The *Uvigerina akitaensis* shells were cleaned using the Cd-cleaning/reductive protocol by Boyle and Keigwin (1985) (Text S3 in Supporting Information S1), while in this study the *Uvigerina* spp. shells were cleaned using the Mg-/oxidative cleaning protocol after Barker et al. (2003) (see Section 2.3). This difference in cleaning protocols leads to Mg-offsets that need to be corrected for (Barker et al., 2003; Elderfield et al., 2012; Pang et al., 2020; Rosenthal et al., 2004). Elderfield et al. (2010) estimate the Mg-offset between these two cleaning protocols in *Uvigerina* spp. to be 0.2 mmol/mol, which was applied to the Mg values in this study to calculate palaeo-temperatures using the above equation. Omitting the Mg-correction would shift the down-core temperature range from between ~0.4 and 8.7°C (see Section 3.2, Figure 4) to between ~2.7 and 10.9°C (without correction).

3. Results

3.1. Age-Depth Relationship for Site U1427 Across the MPT

A shipboard age-depth relationship for Site U1427 was established using seven biostratigraphic tie points and one palaeomagnetic boundary between 250 and 550 m CCSF-D_Patched (Tada et al., 2015b). Recently, two well-dated tephra layers as well as 13 occurrences of warm-water species (indicating the interglacial inflow of the TWC) and low b*/δ^{18}O intervals (indicating glacial maxima) were identified in the sediment cores (see, Text S1–S4 and Table S1 in Supporting Information S1) (Sagawa et al., 2018). Based on the combination of all available chronological markers, sedimentation rates across the MPT were calculated to have varied between ~10 and 75 cm/ka, on average ~50 cm/ka, with the investigated interval spanning from ~680 to 1256 ka (Figure 2).

3.2. Coherence Between b*, Foraminiferal δ^{18}O and Marine Isotope Stages

The newly generated *Uvigerina* spp.-based δ^{18}O record presented in this study, encompasses the MPT (Figure 3). Combining this δ^{18}O record with the revised age-depth relationship (Figure 2 and Text S1 in Supporting Information S1) and the sediment color reflectance index, b* (Figure 3a), enabled the identification of most marine isotope stages encompassing MIS 17-39 through comparison with the LR04-stack (Figure 3b). Across MIS 17-24 glacials are associated with low b* and low δ^{18}O values, corroborating with previous studies from the JS, including the upper ~350 m CCSF-D_Patched of sediment cores at Site U1427 (Figure S4 in Supporting Information S1; Sagawa et al., 2018), while in sediments older than MIS 25 the relationship between b*, δ^{18}O and glacial-interglacial cycles is less clear. Often glacial b* and δ^{18}O run opposite, i.e., showing low b* and relatively high δ^{18}O, with prominent examples being MIS 26, 36 and 38 (Figure 3a).

The identification of the early-MPT high δ^{18}O glacials (older than MIS 25) is supported by lower Mg/Ca temperature estimates (Figures 4b and 4c; Text S3 in Supporting Information S1). The Mg/Ca record varies between ~0.8 and 1.6 mmol/mol (Figure 4b) and covers the intervals ~300–395 m (MIS 19-27) and ~460–525 m CCSF-D_Patched (MIS 35-39), where b* and δ^{18}O show pronounced contrasting relationships (Figure 3a/4a). Temperature estimates (basd on the newly generated Mg/Ca-temperature calibration for JS *Uvigerina akitaensis*, see Text S3 in Supporting Information S1) across MIS 25 to 39 show relatively higher temperatures during suggested interglacials and relatively lower temperatures during suggested glacials, ranging overall between ~0.4 and 8.7°C (Figure 4c). While the absolute temperatures might need to be treated carefully (see Text S3 in Supporting Information S1), their relative changes confirm the identification of glacials/interglacials, hence confirming the switch in the expression of glacials in δ^{18}O across the MPT. Some deviations from this trend, such as low temperatures during the onset of interglacials MIS 37 and 21 are observed but, taken together, the foraminiferal carbonate-based Mg/Ca ratios and δ^{18}O suggest persistent high glacial δ^{18}O values across most glacials of MIS 39-25, often reaching values similar to those of open ocean sites, and lower glacial δ^{18}O values between MIS 24-17 (see Figure 3). This trend continues upwards to the most recent glacial sediments (Figure S4a in Supporting Information S1; Sagawa et al., 2018).

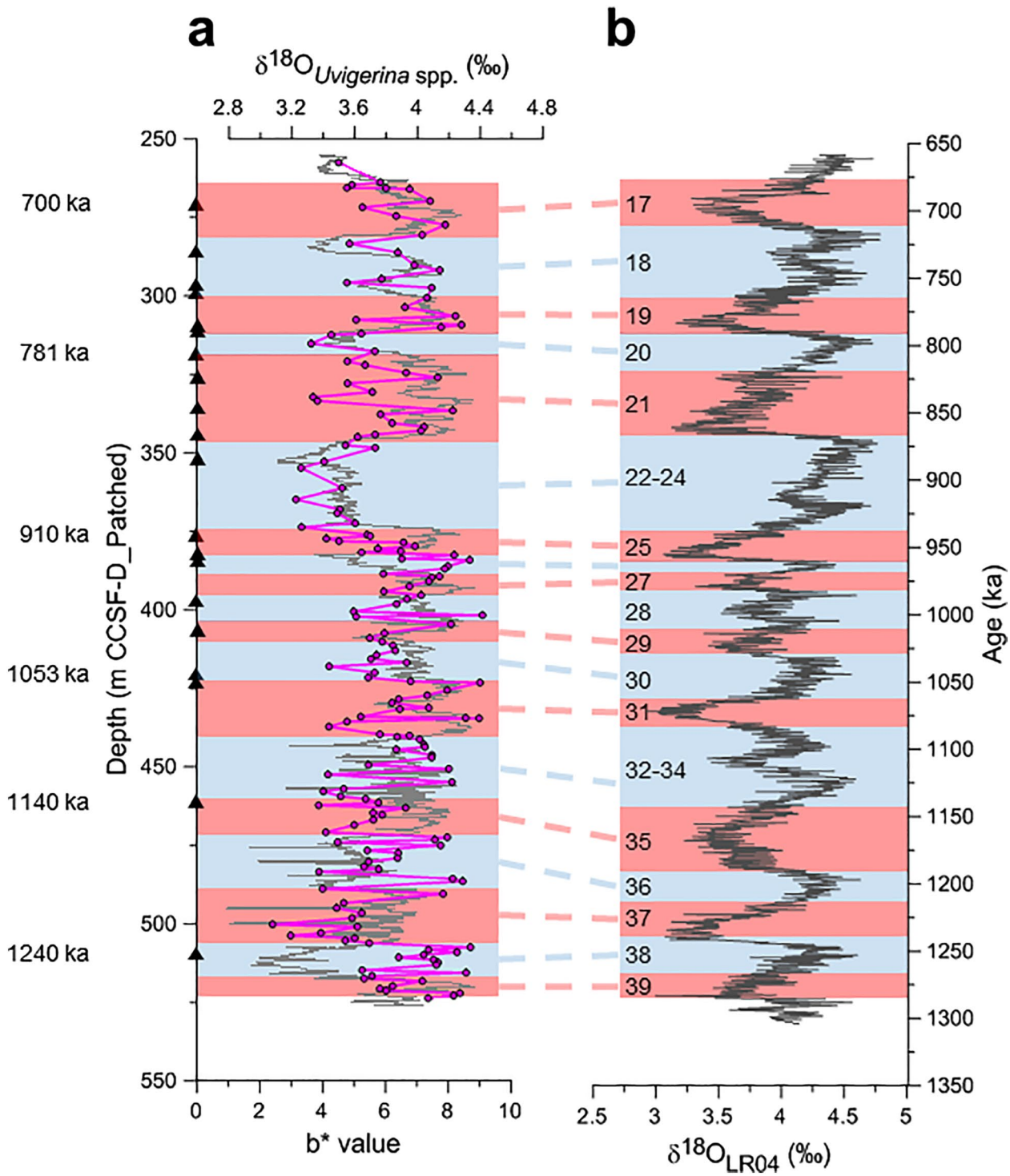

Figure 3. Foraminiferal $\delta^{18}O_{Uvigerina\ spp.}$ record (pink) with color reflectance index, b* (gray), and age-tie points (black triangles on the depth scale) and selected labels for reference (Table S1 in Supporting Information S1) (Figure 3a) compared with the LR04-stack (Lisiecki & Raymo, 2005) (Figure 3b).

4. Discussion

4.1. What Caused the Shift in the Relationship of $\delta^{18}O$ With Glacial-Interglacial Cycles Across the MPT?

The relationship of $\delta^{18}O$ with glacial-interglacial cycles appears to change across the MPT, and the persistent and relatively high glacial $\delta^{18}O$ values across MIS 39-25 suggest an improved water mass exchange with the open

ocean, defying the impact of low saline/low $\delta^{18}O$ waters accumulating around Site U1427. While this effect may be related to the increased amplitudes of glacial sea-level fluctuations across the MPT, we also tested other potential causes of the shift by analyzing the foraminifera shells used for diagenetic alterations and regional variations in precipitation and tectonics across the MPT, which are summarized here.

Diagenesis of foraminifera shells can alter their $\delta^{18}O$ values, leading to deviations from the original signal. We combined high-resolution microscopy with semi-quantitative chemical composition of the shells but found little indication for diagenetic alterations (Text S2 in Supporting Information S1). Furthermore, diagenesis should have had a neglectable effect on the $\delta^{18}O$ record due to using benthic foraminifera, which calcify their shells in a similar environment in which diagenesis takes place (*c.f.* Edgar et al., 2015; Sexton & Wilson, 2009), and due to the fine-grained lithology (predominantly silty clays; Tada et al., 2015b) with continuously high sedimentation rates of up to 75 cm/ka (Figure 2, Table S1 in Supporting Information S1).

Changes in the amount of freshwater input to the JS, influenced by variations in the East Asian summer monsoon, could also have caused the glacial $\delta^{18}O$ shift. Reduced precipitation (as the result of a weaker monsoon), would have reduced the amount of low saline/low $\delta^{18}O$ water runoff and input into the JS, leading to a weakened imprint on the $\delta^{18}O$ records at Site U1427, and consequently higher glacial $\delta^{18}O$ values. However, for MIS 39-25 monsoon proxy records suggest relatively higher glacial precipitation than during MIS 24-17. For example, pollen, spore and vegetation records from southern and central Japan indicate regional climate became warmer and wetter from ~MIS 38 onwards, as inferred from the expansion of broadleaved-tree dominated temperate warm forests (Fujiki & Ozawa, 2008; Kitaba et al., 2012). From MIS 24, plants indicative of cooler and, more importantly, dryer conditions start to dominate during glacials (Kitaba et al., 2012). Similarly, mineralogical and facies studies of deposits on the Chinese Loess Plateau, controlled by variations in the monsoon and leading to pedogenesis and the deposition of paleosol at times of strong East Asian summer monsoon precipitation and loess layers at times of relatively weaker summer monsoon and stronger winter monsoon winds, revealed a significant precipitation increase starting around 1200 ka (~MIS 36), affecting glacials more significantly than interglacials (An et al., 1990; Han et al., 2012; Meng et al., 2018; Peng et al., 2020). Most intriguingly, precipitation is suggested to have been at a similarly low level (~30 mm/a) during MIS 38 and 22 (Peng et al., 2020), two glacials with distinctively different $\delta^{18}O$ characterization (Figure 4a). These variabilities in precipitation and freshwater input across the MPT are also indicated by the $\delta^{18}O$ values of the surrounding seawater (Text S4 and Figure S4c in Supporting Information S1), a record not been shown before for the JS.

These findings imply that processes other than preservation state/diagenesis and/or regional precipitation must have been involved to explain the shift in glacial $\delta^{18}O$, most likely a change in the palaeoceanography of the shallow, southern JS. The shift from high-$\delta^{18}O$ (open ocean-like) glacials across MIS 39-25 to low-$\delta^{18}O$ (restricted JS) glacials from MIS 24 onwards could have been caused by local tectonic uplift movements. Although the study site is located in a tectonically very active region with volcanic events having taken place in southern Japan and the Japanese Isles across the MPT, no local uplift events could be identified (Itaki, 2016; Kitamura & Kawagoe, 2006; Yoon, 1997). The biggest tectonic events around the TSS are related to the opening of the JS, starting in the late Oligocene, with stress field changes (extensional to compressional) during the mid-Miocene and, although minor movements (minor faulting) took place after the mid-Miocene, the TSS area has been tectonically stable since the mid-Miocene, which is supported by modern seismological activity (Claringbould et al., 2019; Fabbri et al., 1996; Ishikawa & Tagami, 1991; Katsura & Nagano, 1976; Son et al., 2015). Although there is a possibility of sill depth changes related to deposition/erosion in the TSS, no large (tectonically induced) sill depth change is expected.

There is strong evidence for increased glacio-eustatic sea-level fluctuations that might have led to an improved glacial connection between the JS and the open ocean across MIS 39-25 and a more restricted JS palaeoceanography across MIS 24-17. Before MIS 25, global eustatic sea-level fluctuations over glacial-interglacial cycles were smaller (on average, glacial sea-level dropped by ~–60 to −80 m between ~2,700 and 1200 ka) than since MIS 22, i.e., during the glacials of the last ~900 ka, where sea-levels dropped to as much as −120m ± 32 m below present (*c.f.* Sosdian & Rosenthal, 2009). While sea-level curves based on foraminiferal $\delta^{18}O$ are not available for the JS because of the widespread glacial carbonate dissolution (see above), they exist for other sites. For example, global sea-level curves modeled from the LR04-stack cover the last ~1100 ka (Bintanja et al., 2005) and, using inverse sea-level modeling, the last 3,600 ka (Berends et al., 2019). Other sea-level curves that encompass MIS 39-17 have been produced from records of Gibraltar in the Mediterranean Sea (Rohling et al., 2014) and from the

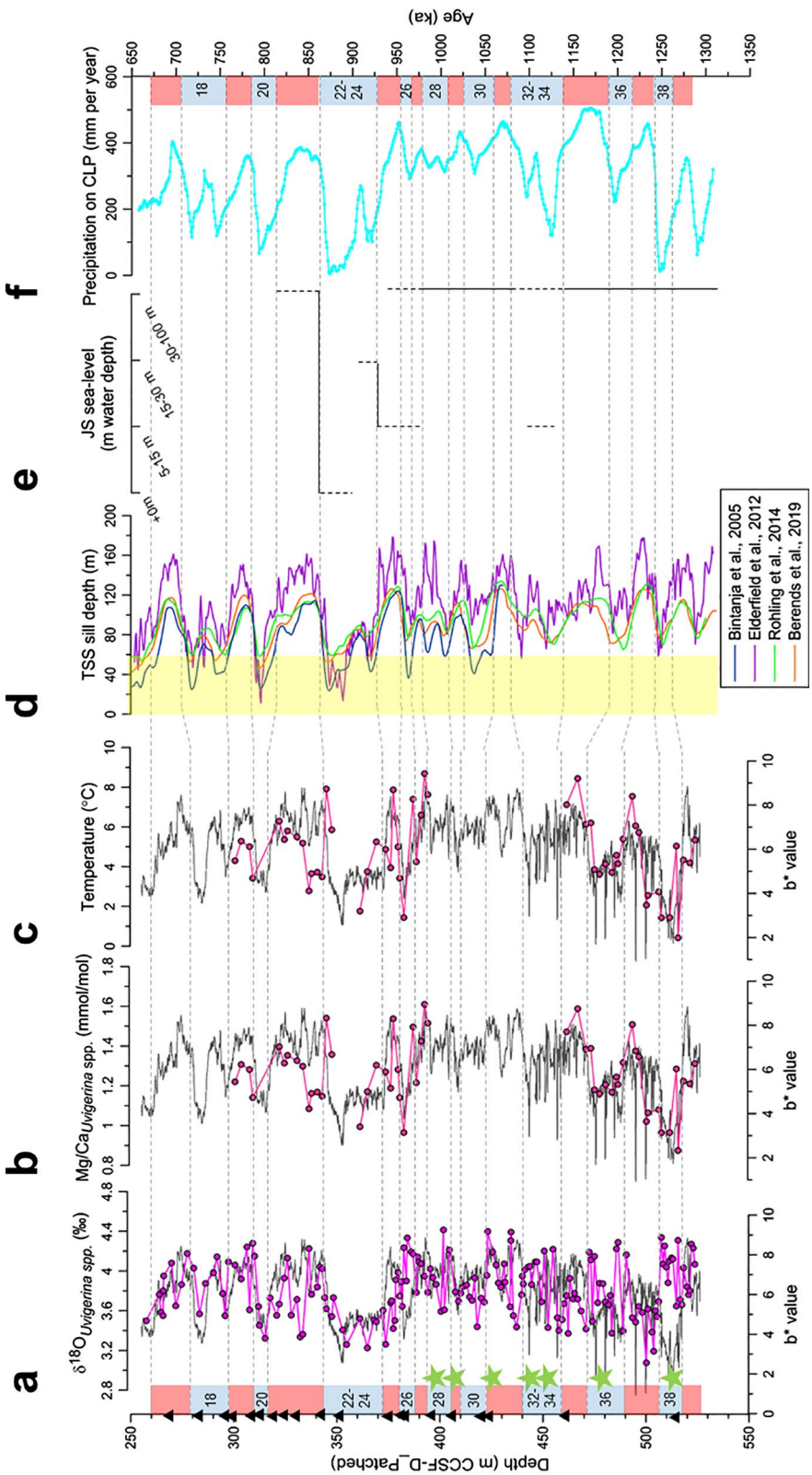

Figure 4. Benthic foraminiferal $\delta^{18}O$ (a) (replotted for reference), Mg/Ca ratios (b) and Mg/Ca-derived temperatures (c) of Site U1427 with b* index (gray) in the background. On the left, glacial intrusions of warm-water species are indicated by green stars (based on Itaki et al., 2018; Kitamura et al., 2001; Tada et al., 2015b), age-tie points by triangles (*c.f.* Tada et al., 2015b; Sagawa et al., 2018) and marine isotope stages by numbers. Compared with TSS sill level stands (calculated from global sea-level reconstructions based on Bintanja et al., 2005; Berends et al., 2019; Elderfield et al., 2012 and Rohling et al., 2014. Yellow area indicating TSS sill stands at which the JS is nearly isolated) (d), JS water depth estimates (based on lithological studies of the Omma Formation in Kanazawa City; Kitamura, 2016) (e) and a precipitation/monsoon intensity reconstruction from the Chinese Loess plateau (Peng et al., 2020) (f).

South West Pacific near New Zealand (Elderfield et al., 2012). Using these sea-level reconstructions, palaeo-water levels over the TSS sill (hereafter referred to as sill depths) were estimated by deducting past sea-level stands from the modern TSS sill depth of 130 m (*c.f.* Oba et al., 1991). The resulting palaeo-sill depths are shown in Figure 4d. All but the Bintanja et al. (2005) curves suggest relatively stable interglacial sill depths/sea-levels, while glacial sill depths were greater across MIS 39-25 than across MIS 24-17, when the TSS sill regularly became as shallow as 50 to 20 m (Figure 4d).

Palaeo-sea-level reconstructions from the JS are limited to lithological and micropalaeontological assemblage studies on the shallow-water deposits of the Omma Formation in outcrops near Kanazawa City, ∼200 km east of Site U1427 (e.g., Hoiles et al., 2012; Kitamura, 1991; Kitamura et al., 2001; Kitamura & Kawagoe, 2006; Kitamura & Kimoto, 2006; Kitamura, 2016). Their lithofacies inventory also suggests higher glacial sea-levels in the JS before MIS 25 (Figure 4e; *op. cit.*). In detail, the Omma Formation lithofacies suggests inflow via the TSS during each interglacial since MIS 56 (∼1700 ka) and that sediments were deposited in a fairly constant water depth of 30 to 100 m during MIS 39–27, while sediments younger than that were deposited under more variable sea-levels (Kitamura, 2016). For example, during MIS 27–23 water depth at the Omma Formation outcrops fell from ∼100 m to between just 5 to 30 m, followed by aerial exposure of the area and the formation of a back marsh environment with trees and mammal footprints during MIS 22, before the return to around 30 to 100 m water depth during MIS 21 and return of marine molluscs (Kitamura, 2016) (Figure 4e). These findings of higher glacial sea-levels, both globally and in the JS, during MIS 39–25 and lower levels across MIS 24–17 suggest the long-term glacio-eustatic sea-level development across the MPT is a most likely cause for the switch in glacial $\delta^{18}O$ at Site U1427, enabling a better water mass exchange with the open ocean before MIS 25 and implying changes in the JS palaeoceanography across the MPT.

4.2. Palaeoceanographic Changes in the Shallow, Southern Japan Sea Across the MPT

The improved glacial water mass exchange between the JS and the open ocean, based on $\delta^{18}O$, has implications for the palaeoceanography of the basin. We propose a new glacial palaeoceanographic mode for the shallow, southern JS across MIS 39-25, characterized by relatively unrestricted water mass exchange encompassing entire glacials. We differentiate **three modes across the MPT**, which are summarized here.

In order to determine the TSS sill depth at which the system switches glacial modes from high, open ocean-like to low, JS-specific $\delta^{18}O$ values, individual glacials must be studied in detail. For example, the glacial of MIS 26 shows high $\delta^{18}O$ values, indicating a good water mass exchange with the open ocean, while MIS 24 shows reduced $\delta^{18}O$ values, indicating a freshwater imprint on the record and, hence, restricted water mass exchange (Figure 4a). During MIS 26 the TSS sill depth was around 100 to 75 m (i.e., sea-level drop of −30 to −55 m) and around 80 to 60 m (sea-level drop of −50 to −70 m) during MIS 24 (Figure 4d). Therefore, at TSS sill stands of greater than 100 m, i.e. sea-level of less than –30 m below present, the $\delta^{18}O$ record is unaffected by the input of low saline/low $\delta^{18}O$ waters due to unrestricted water mass exchange between the JS and the open ocean (**mode 1** in Figure 5a). Palaeoceanographic mode 1 prevails during interglacials across MIS 39-17 and encompasses mode 4 in Tada et al. (1999) and mode 3 in Saavedra-Pellitero et al. (2019). At intermediate TSS sill stands between 100 and ∼60 m, i.e. sea-level is about –30 to –70 m below present, water mass exchange with the open ocean is restricted and the varying contributions of ECSCW (low saline/low $\delta^{18}O$, warm, nutrient-rich) has a strong influence on freshwater imprints on $\delta^{18}O$; this is proposed **mode 2** (Figure 5b). The influence of varying ECSCW contributions to the TWC can be demonstrated by comparing, for example, the interglacial MIS 23 and the glacials 38, 36 and 30. During MIS 23 TSS sill stands are around 80 to 90 m and $\delta^{18}O$ is low (Figures 4a and 4d), indicating restricted inflow via the TSS and relatively high contributions of ECSCW to the TWC, as can also be inferred from high fluxes in marine productivity proxies as a result of the enhanced nutrient input by the ECSCW (Felder et al., 2021) and a relatively high precipitation on the Chinese Loess Plateau (Figure 4f). In contrast, during MIS 38 TSS sill levels were at times shallower than during MIS 23, dropping to as little as ∼60 m, but $\delta^{18}O$ is consistently high, suggesting a relatively good water mass exchange with the open ocean and reduced contributions of ECSCW, as can also be inferred from relatively lower marine productivity (Felder et al., 2021) and much lower precipitation on the Chinese Loess Plateau (Figures 4a–4d, 4f).

The glacials of MIS 30 and 36 are other another examples of the sensitivity of mode 2 to variations in the East Asian summer monsoon are the glacials of MIS 36 and 30. MIS 36 begins and ends with relatively high $\delta^{18}O$

10.1029/2021PA004236

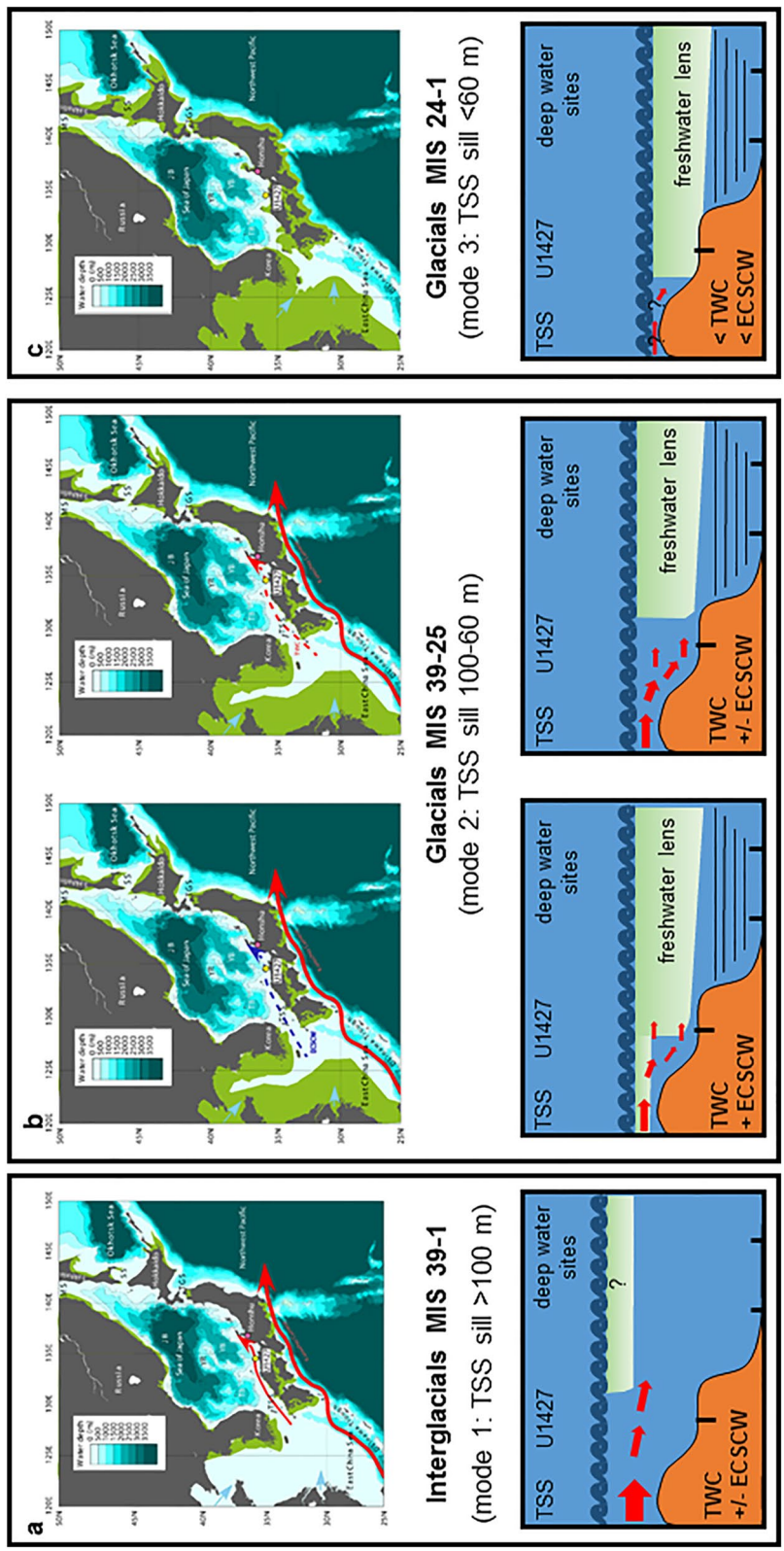

Figure 5. Palaeoceanographic modes for the shallow, southern Japan Sea across the MPT with TSS sill depths (top row), showing mode 1 (a), the stages of mode 2 (b) and mode 3 (c). Below are schematic illustrations of the circulation in the southern Japan Sea during each stage. Base map of the top row from Tada et al. (2013), with palaeo-shorelines redrawn from Saavedra-Pellitero et al. (2019) (using mode 1 sea-level at −100 m and mode 3 sea-level at −20 m below present), from Tada et al. (2013) for central to north Honshu, Hokkaido and Sakhalin (mode 2) and from Park and Chu (2006) for southern Japan Sea, East China Sea and TSS area (mode 2 sea-level at −75 m below present). Vertical lines in bottom row indicate drill sites, horizontal lines in b and c indicate stratified water column. TSS, Tsushima strait; TWC, Tsushima warm current; CSCW, East China Sea coastal water.

and lower $\delta^{18}O$ values in its mid-section, while MIS 30 has overall low $\delta^{18}O$ values (Figure 4a). During MIS 36, the reduced $\delta^{18}O$ values are likely associated with a period of increased monsoon precipitation affecting the $\delta^{18}O$ record and, although a direct proxy for freshwater input/monsoon variations (such as diatom assemblages) is not available, the enhanced contributions of nutrient-rich ECSCW can also be inferred from enhanced marine productivity (Felder et al., 2021) and high precipitation over the Chinese Loess Plateau (Figure 4f). During MIS 30, the low $\delta^{18}O$ values may be the result of a combination of enhanced monsoon precipitation (Figure 4f) and potentially a sea-level/sill level that would have reduced the exchange of water masses with open ocean (Figure 4d, yellow area). Comparing the proposed mode 2 with previous stuides, it encompasses modes 2 and 3 of Tada et al. (1999) and mode 2 of Saavedra-Pellitero et al. (2019). Mode 2 dominates during glacials of MIS 39-25, strongly suggesting a consistent glacial connection/water mass exchange between the open ocean and the shallow, southern JS during the early stages of the MPT. Further evidence for the glacial inflow via the TSS comes from numerous micropalaeontological studies highlighting the (intermittent) presence of warm-water species, having originated from the East China Sea and having been identified in outcrops and marine sediments from the JS across glacials of MIS 39-25. For example, micropalaeontological studies on the Omma Formation describe the occasional glacial occurrence of the warm water foraminifera *Globigerinoides ruber* (d'Orbigny, 1839) in sediments equivalent in time to MIS 38, 36 and 34 (Hoiles et al., 2012; Kitamura et al., 2001). *Globigerinoides ruber* have also been identified at Site U1427 in sediments depths corresponding to MIS 38 and 39 (Tada et al., 2015b). Furthermore, radiolarian assemblages contain warm water species at depths corresponding to MIS 34, 32, 28 and potentially further glacials, although these depths cannot be dated with great certainty based on the data provided (Itaki et al., 2018). While these studies indicate the occasional inflow of warm waters via the TSS, the continuous $\delta^{18}O$ record of Site U1427 suggests a persistent glacial inflow or water mass exchange across MIS 39-25.

The third proposed palaeoceanographic mode (**mode 3**) occurs at lowest TSS sill/sea-level stands of less than 60 m, i.e. sea-levels lower than –70 m below present (yellow in Figure 4d). During mode 3 water mass exchange with the open ocean is restricted and the JS becomes nearly isolated, leading to the formation of a low-saline surface layer which impacts on the $\delta^{18}O$ record, leading to lower values (Figure 5c). This mode encompasses mode 1 in Tada et al. (1999) and Saavedra-Pellitero et al. (2019), and it persists during glacials across MIS 24-17, continuing upwards to the most recent sediments (Figure S4 in Supporting Information S1; Sagawa et al., 2018). Intriguingly, the switch from glacials dominated by mode 1 to predominantly mode 3 first appears during the glacial of MIS 24 (sea-level about ~90 to 100 m below present; *c.f.* Bintanja et al., 2005; Elderfield et al., 2012), a time which is crucial in the MPT as the modern 100 ka frequency in glacial-interglacial climate cyclicity becomes statistically significant in marine $\delta^{18}O$ records (e.g., Clark et al., 2006; Imbrie et al., 1992; Kitaba et al., 2011; Sosdian & Rosenthal, 2009). Previously published sea-level reconstructions suggest a significant sea-level fall of up to ~120 m below present not before MIS 22 (Figure 3d; Berends et al., 2019; Bintanja et al., 2005; Elderfield et al., 2012; Haq et al., 1987; Lisiecki & Raymo, 2005; Rohling et al., 2014; Sosdian & Rosenthal, 2009), associated with declining temperatures and significant ice-volume increase around 900 ka (themed the "900 ka-event"; e.g., Elderfield et al., 2012; Farmer, Hönisch, et al., 2019; Hoogakker et al., 2006; Raymo et al., 1997; Rohling et al., 2014). The $\delta^{18}O$-mode switch at Site U1427 precedes the 900 ka-event by one glacial, demonstrating the great sensitivity of the sediments of Site U1427 to sea-level fluctuations across the MPT.

There may be consequences for dating JS deep-water sediments should the improved glacial water mass exchange, as suggested by mode 2, extend to greater water depths. The inflow via the TSS, i.e., the TWC with variable amounts of ECSCW, affects water mass stratification and the lithology at deep-water sites from the JS (see Introduction), leading to the deposition of dark and light sediment layers, which have been associated with glacials and interglacials respectively (e.g., Oba et al., 1991; Tada et al., 1999). Hypothetically, the improved glacial water mass exchange that led to higher glacial $\delta^{18}O$ values at Site U1427, could have extended further offshore to be located above deep-water sites. Here the more saline/higher $\delta^{18}O$ waters could avert water column stratification, to some degree, and hence improve carbonate preservation at deep-water sites, leading to lighter colors of glacial sediments. As the inflow from the south/East China Sea is, in addition, likely warmer than JS waters, warm water species could be contained in the glacial sediments. Therefore, if the effect of the glacial TWC inflow would have continued to greater water depths, it would lead to some difficulties in sediment dating, as the assumption of light sediments with warm-water microfossils indicating interglacials, may be invalid.

5. Conclusions and Implications

This study shows that there are changes in the JS palaeoceanography across the MPT, which have not been observed previously but may have implications for the interpretation of dark/light sediment alternations from JS deep-water sites, commonly associated with interglacials and glacials respectively (e.g., Oba et al., 1991; Tada et al., 1999). The $\delta^{18}O$ record of Site U1427, encompassing MIS 39-17, shows a switch in the expression of glacials in $\delta^{18}O$ across the MPT, associated with higher glacial sea-levels before MIS 25, globally and in the JS. An improved glacial water mass exchange between the shallow, southern JS and the open ocean is proposed as the cause of the $\delta^{18}O$ switch, having attenuated any potential freshwater imprint on $\delta^{18}O$ and resulting in relatively higher glacial $\delta^{18}O$ values across MIS 39-25 than across MIS 24-17, and continuing upwards to the most recent sediments (Figure S4a in Supporting Information S1; Sagawa et al., 2018). Deviations from this trend are likely associated with enhanced monsoon precipitation, for example, lower $\delta^{18}O$ values during the mid-section of MIS 36 (Figure 4), and demonstrate the sensitivity of the sediments of Site U1427 to orbital- and sub-orbital scale monsoon variations. In contrast to previous studies that suggest the possibility of an intermittent glacial TWC inflow during some glacials, the new proposed mode suggests inflow was possible for the duration of entire glacials across MIS 39-25. Should this mode have extended further offshore and to greater water depths, it may have significant consequences for the dating of JS deep-water sediments, as the interpretation of light layers with warm-water species present as representing interglacials, may not be valid. Crucially, the $\delta^{18}O$-mode switch from glacials with TWC inflow to such glacials suggesting the (near) isolation of the JS, occurs at MIS 25/24. This is one glacial-interglacial cycle earlier than the significant ice-volume increase and associated sea-level fall identified in open ocean sites (i.e., 900 ka-event; e.g., Elderfield et al., 2012). This demonstrates the great sensitivity of the sediments of Site U1427 to glacio-eustatic sea-level variations and suggests that significant events took place before the 900 ka-event, which should be considered when deciphering the mechanisms surrounding the MPT.

Conflict of Interest

The authors declare no conflicts of interest relevant to this study.

Data Availability Statement

All new data, shown in the manuscript and its supporting information, are included in the open-access data repository PANGAEA (https://doi.pangaea.de/10.1594/PANGAEA.931921).

Acknowledgments
This study used samples provided by the Integrated Ocean Drilling Program (IODP). We would like to thank the co-chiefs, Ryuji Tada and Richard W. Murray, and all IODP Expedition 346 participants, and two anonymous reviewers for their insights and tremendous efforts to improve this manuscript. This research was supported by a NERC IAPETUS Doctoral Training Partnership studentship (NE/L002590/1) and by a British Geological Survey CASE partnership (BUFI S270) and forms part of S. Felder's PhD research ("The mid-Pleistocene climate transition in the Japan Sea: Insights of a combined palaeoceanographic and -monsoon, multi-proxy study using marine sediments of IODP Site U1427 from the shallow, southern Japan Sea", unpublished PhD thesis, Newcastle University, UK). Analyses were also supported by the National Environmental Isotope Facility at the British Geological Survey under awards IP-16668-111, IP-1486-1114 and IP-1668-1116, and by a research grant by the European Consortium for Ocean Research Drilling (ECORD) to undertake training and analysis in the Mg/Ca determination at the Godwin Laboratory, Cambridge. This work is also partly supported by JSPS Grant JPMXS05E2900001 and by Kanazawa University SAKIGAKE project 2020. We are grateful to UK IODP for supporting S. Felder in the participation in the Expedition 346 second post cruise meeting in Melbourne, Australia, and for A. C. G. Henderson in Expedition 346 (NE/L002655/1). We would also like to thank Dr Tracy Ace, University of Leeds, for making microscope facilities available as well as Christian März and Eva for their continuous support and patience during the lead author's PhD and the writing this manuscript. Each named author has substantially contributed to conducting the underlying research and drafting this manuscript.

References

An, Z., Tunghseng, L., Yanchou, L., Porter, S. C., Kukla, G., Xihao, W., et al. (1990). The long-term paleomonsoon variation recorded by the loess-paleosol sequences in central China. *Quaternary International*, *7/8*, 91–95. https://doi.org/10.1016/1040-6182(90)90042-3

Barker, S., Greaves, M., & Elderfield, H. (2003). A study of cleaning procedures used for foraminiferal Mg/Ca paleothermometry. *Geochemistry, Geophysics, Geosystems*, *4*(9), 8407. https://doi.org/10.1029/2003gc000559

Berends, C. J., de Boer, B., Dolan, A. M., Hill, D. J., & van de Wal, R. S. W. (2019). Modelling ice sheet evolution and atmospheric CO_2 during the late Pliocene. *Climate of the Past*, *15*, 1603–1619. https://doi.org/10.5194/cp-15-1603-2019

Bintanja, R., van de Wal, R. S. W., & Oerlemans, J. (2005). Modelled atmospheric temperatures and global sea levels over the past million years. *Nature*, *437*, 125–128. https://doi.org/10.1038/nature03975

Black, H. D., Anderson, W. T., & Alvarez-Zarikian, C. A. (2018). Data report: Organic matter, carbonate, and stable isotope stratigraphy from IODP Expedition 346 Sites U1426, U1427, and U1429. In R. Tada, R. W. Murray, C. A. Alvarez Zarikian (Eds.), *Proceedings of IODP expedition 346*. Integrated Ocean Drilling Program. https://doi.org/10.2204/iodp.proc.346.204.2018

Boyle, E., & Keigwin, L. (1985). Comparison of Atlantic and Pacific paleochemical records for the last 215,000 years: Changes in deep ocean circulation and chemical inventories. *Earth and Planetary Science Letters*, *76*, 135–150. https://doi.org/10.1016/0012-821x(85)90154-2

Chalk, T. B., Hain, M. P., Foster, G. F., Rohling, E. J., Sexton, P. F., Badger, M. P. S., et al. (2017). Causes of ice age intensification across the mid-Pleistocene transition. *Proceedings of the National Academy of Sciences of the USA*, *114*(50), 13114–13119. https://doi.org/10.1073/pnas.1702143114

Cheng, H., Edwards, R. L., Sinha, A., Spötl, C., Yi, L., Chen, S., et al. (2016). The Asian monsoon over the past 640,000 years and ice age terminations. *Nature*, *534*, 640–646. https://doi.org/10.1038/nature18591

Claringbould, J. S., Sato, H., Ishiyama, T., Van Horne, A., Kawasaki, S., & Abe, S. (2019). *Cenozoic evolution of the Tsushima Strait and the Fukue Basin, southern Sea of Japan: An interplay of tectonics, palaeo-environment, and volcanism*. Japan Geoscience Union Meeting. Abstract SCG57-12, 26th–30th May 2019.

Clark, P. U., Alley, R. B., & Pollard, D. (1999). Northern hemisphere ice-sheet influences on global climate change. *Science*, *286*, 1104–1111. https://doi.org/10.1126/science.286.5442.1104

Clark, P. U., Archer, D., Pollard, D., Blum, J. D., Rial, J. A., Brovkin, V., et al. (2006). The middle Pleistocene transition: Characteristics, mechanisms, and implications for long-term changes in atmospheric CO_2. *Quaternary Science Reviews*, *25*, 3150–3184. https://doi.org/10.1016/j.quascirev.2006.07.008

Clemens, S. C., Holbourn, A., Kubota, Y., Lee, K. E., Liu, Z., Chen, G., et al. (2018). Precession-band variance missing from East Asian monsoon runoff. *Nature Communications*, *9*, 3364. https://doi.org/10.1038/s41467-018-05814-0

Clemens, S. C., Prell, W. L., & Sun, Y. (2010). Orbital-scale timing and mechanisms driving late Pleistocene Indo-Asian summer monsoons: Reinterpreting cave speleothem $\delta^{18}O$. *Paleoceanography*, *25*, PA4207. https://doi.org/10.1029/2010pa001926

De Villers, S., Greaves, M., & Elderfield, H. (2002). An intensity ratio calibration method for the accurate determination of Mg/Ca and Sr/Ca of marine carbonates by ICPAES. *Geochemistry, Geophysics, Geosystems*, *3*, GC000169.

DeMenocal, P. B. (1995). Plio-Pleistocene African climate. *Science*, *270*(5233), 53–59. https://doi.org/10.1126/science.270.5233.53

D′Orbigny, A. D. (1839). Foraminifères. In R. De la Sagra (Ed.), *Histoire physique, politique et naturelle de l'ile de Cuba* (pp. 82). Royal Geographical Society.

Dunbar, R. B., DeMenocal, P. B., & Burckle, L. (1992). 26. Late Pliocene-Quaternary biosiliceous sedimentation rate at site 798, Japan Sea. In K. A. Pisciotto, J. C. Ingle, M. T. von Breymann, J. Barron, et al. (Eds.), *Proceedings of ODP, scientific results* (Vol. 127/128, pp. 439–455).

Edgar, K. M., Anagnostou, E., Pearson, P. N., & Foster, G. L. (2015). Assessing the impact of diagenesis on $\delta^{11}B$, $\delta^{13}C$, $\delta^{18}O$, Sr/Ca and B/Ca values in fossil planktonic foraminiferal calcite. *Geochimica et Cosmochimica Acta*, *166*, 189–209. https://doi.org/10.1016/j.gca.2015.06.018

Elderfield, H., FerrettiGreaves, P. M., Crowhurst, I. N., Mc Cave, I. N., Hodell, D., Piotrowski, A. M., et al. (2012). Evolution of ocean temperature and ice volume through the mid-Pleistocene climate transition. *Science*, *337*, 704–709. https://doi.org/10.1126/science.1221294

Elderfield, H., & Ganssen, G. (2000). Past temperature and $\delta^{18}O$ of surface ocean waters inferred from foraminiferal Mg/Ca ratios. *Nature*, *405*, 442–445. https://doi.org/10.1038/35013033

Elderfield, H., Greaves, M., Barker, S., Hall, I., Tripati, A., Ferretti, P., et al. (2010). A record of bottom water temperature and seawater $\delta^{18}O$ for the southern ocean over the past 440 kyr based on Mg/Ca of benthic foraminiferal *Uvigerina* spp. *Quaternary Science Reviews*, *29*, 160–169. https://doi.org/10.1016/j.quascirev.2009.07.013

Elderfield, H., Yu, J., Anand, P., Kiefer, T., & Nyland, B. (2006). Calibrations for benthic foraminiferal Mg/Ca paleothermometry and the carbonate ion hypothesis. *Earth and Planetary Science Letters*, *250*, 633–649. https://doi.org/10.1016/j.epsl.2006.07.041

Fabbri, O., Charvet, J., & Fournier, M. (1996). Alternate senses of displacement along the Tsushima fault system during the Neogene based on fracture analyses near the western margin of the Japan Sea. *Tectonophysics*, *257*, 275–295. https://doi.org/10.1016/0040-1951(95)00151-4

Farmer, J. R., Goldstein, S. L., Haynes, L. L., Hönisch, B., Kim, J., Pena, L., et al. (2019). Data constraints on ocean-carbon cycle feedbacks at the mid-Pleistocene transition. *Past Global changes Magazine*, *27*(2), 62–63.

Farmer, J. R., Hönisch, B., Haynes, L. L., Kroon, D., Jung, S., Ford, H. L., et al. (2019). Deep Atlantic Ocean carbon storage and the rise of 100,000-year glacial cycles. *Nature Geoscience*, *12*, 355–360. https://doi.org/10.1038/s41561-019-0334-6

Felder, S., Henderson, A. C. G., Leng, M. J., & Sloane, H. J. (2021). Data report: Bulk sediment organic matter, carbonate, and stable isotope stratigraphy from IODP expedition 346 site U1427 (250 m to 530 m CCSF-D_Patched). In R. Tada, R. W. Murray, C. A. Alvarez Zarikian (Eds.), *Proceedings of IODP expedition 346*. Integrated Ocean Drilling Program.

Fujiki, T., & Ozawa, T. (2008). Vegetation change in the main island of Okinawa, southern Japan from late Pliocene to early Pleistocene. *Quaternary International*, *184*, 75–83. https://doi.org/10.1016/j.quaint.2007.09.009

Gallagher, J. S., Sagawa, T., Henderson, A. C. G., Saavedra-Pellitero, M., De Vleeschouwer, D., Black, H., et al. (2018). East Asian monsoon history and paleoceanography of the Japan Sea over the last 460,000 years. *Paleoceanography and Paleoclimatology*, *33*, 683–702. https://doi.org/10.1029/2018pa003331

Greaves, M., Caillon, N., Rebaubier, H., Bartoli, G., Bohaty, S., Cacho, I., et al. (2008). Interlaboratory comparison study of calibration standards for foraminiferal Mg/Ca thermometry. *Geochemistry, Geophysics, Geosystems*, *9*(8), GC001974. https://doi.org/10.1029/2008gc001974

Han, W., Fan, X., & Berger, A. (2012). Tibet forcing of mid-Pleistocene synchronous enhancement of East Asian winter and summer monsoons revealed by Chinese loess record. *Quaternary Research*, *78*, 174–184. https://doi.org/10.1016/j.yqres.2012.05.001

Haq, B. U., Hardenbol, J., & Vail, P. R. (1987). Chronology of fluctuating sea levels since the Triassic. *Science*, *235*, 1156–1167. https://doi.org/10.1126/science.235.4793.1156

Hasenfratz, A. P., Jaccard, S. L., Martínez-García, A., Sigman, D. M., Hodell, D. A., Vance, D., et al. (2019). The residence time of Southern Ocean surface waters and the 100,000 year ice age cycle. *Science*, *363*, 1080–1084. https://doi.org/10.1126/science.aat7067

Hathorne, E. C., Gagnon, A., Felis, T., Adkins, J., Asami, R., Boer, W., et al. (2013). Interlaboratory study for coral Sr/Ca and other element/Ca ratio measurements. *Geochemistry, Geophysics, Geosystems*, *14*, 3730–3750. https://doi.org/10.1002/ggge.20230

Hays, J. D., Imbrie, J., & Shackleton, N. J. (1976). Variations in the Earth's orbit: Pacemakers of the ice ages. *Science*, *194*(4270), 1121–1132. https://doi.org/10.1126/science.194.4270.1121

Higgins, J. A., Kurbatov, A. V., Spaulding, N. E., Brook, E., Introne, D. S., Chimiak, L. M., et al. (2015). Atmospheric composition 1 million years ago from blue ice in the Allan Hills, Antarctica. *Proceedings of the National Academy of Sciences of the USA*, *112*, 6887–6891. https://doi.org/10.1073/pnas.1420232112

Hoiles, P. W., Gallagher, S. J., Kitamura, A., & Southwood, J. M. (2012). The evolution of the Tsushima current during the early Pleistocene in the Sea of Japan: An example from marine isotope stage (MIS) 47. *Global and Planetary Change*, *92–93*, 162–178. https://doi.org/10.1016/j.gloplacha.2012.05.015

Hönisch, B., Hemming, N. G., Archer, D., Siddall, M., & McManus, J. F. (2009). Atmospheric carbon dioxide concentration across the mid-Pleistocene transition. *Science*, *324*, 1551–1554. https://doi.org/10.1126/science.1171477

Hoogakker, B. A. A., Rohling, E. J., Palmer, M. R., Tyrrell, T., & Rothwell, R. G. (2006). Underlying causes for long-term global ocean $\delta^{13}C$ fluctuations over the last 1.20 Myr. *Earth and Planetary Science Letters*, *248*, 15–29. https://doi.org/10.1016/j.epsl.2006.05.007

Ikehara, K. (1991). Modern sedimentation off San'In district in the southern Japan Sea. In K. Takano (Ed.), *Oceanography of asian marginal seas*. *Elsevier oceanography series 54* (pp. 143–161). Elsevier Science Publishers. https://doi.org/10.1016/s0422-9894(08)70092-8

Ikehara, K., Kikawa, K., Katayama, H., & Seto, K. (1994). Late Quaternary paleoceanography of the Sea of Japan; a tephrochronological and sedimentological study. In E. H. Juvigne (Ed.), *Quaternary environmental changes. Proceedings of the 29th international geological congress. (Part B)* (pp. 229–235).

Imbrie, J., Boyle, E., Clemens, S., Duffy, A., Howard, W., Kukla, G., et al. (1992). On the structure and origin of major glaciation cycles – 1. Linear responses to Milankovitch forcing. *Paleoceanography*, *7*, 701–738. https://doi.org/10.1029/92pa02253

Imbrie, J., Boyle, E., Clemens, S., Duffy, A., Howard, W., Kukla, G., et al. (1993). On the structure and origin of major glaciation cycles – 2. The 100,000 year cycle. *Paleoceanography*, *8*, 699–735. https://doi.org/10.1029/93pa02751

Ingle, J. C. (1975). Pleistocene and Pliocene foraminifera from the Japan Sea, leg 31, Deep Sea Drilling Project. In D. E. Karig, J. C. Ingle, A. H. Bouma, C. H. Ellis, N. Haile, I. Koizumi, et al. (Eds.), *Initial report of the deep sea drilling project* (Vol. 31, pp. 693–701). Ocean Drilling Program. https://doi.org/10.2973/dsdp.proc.31.1975

Ingle, Jr, J. C., Bristow, J. S., Bruckle, L. H., Charvet, J., Cragg, B. A., deMenocal, P., et al. (1990). Site 798, In J. C. Ingle, Jr, K. Suyehiro, M. T. von Breymann, J. S. Bristow, L. H. Burckle, J. Charvet, et al. (Eds.), *Initial report of the Ocean Drilling Program* (Vol. 128, pp. 121–236). Ocean Drilling Program.

Inoue, Y. (1989). *Northwest Pacific foraminifera as paleoenvironmental indicators. Science Reports of the Institute of Geoscience* (Vol. 10, pp. 57–98). University of Tsukuba, Section B: Geological Sciences. https://doi.org/10.1016/s0074-7696(08)61334-0

Irino, T., Tada, R., Ikehara, K., Sagawa, T., Karasuda, A., Kurokawa, S., et al. (2018). Construction of perfectly continuous records of physical properties for dark-light sediment sequences collected from the Japan Sea during Integrated Ocean Drilling Program expedition 346 and their potential utilities as paleoceanographic studies. *Progress in Earth and Planetary Sciences*, *5*, 23. https://doi.org/10.1186/s40645-018-0176-7

Ishikawa, N., & Tagami, T. (1991). Paleomagnetism and fission-track geochronology on the Goto and Tsushima Islands in the Tsushima Strait area: Implications for the opening mode of the Japan Sea. *Journal of Geomagnetism and Geoelectricity*, *43*, 229–253. https://doi.org/10.5636/jgg.43.229

Ismail-Zadeh, A., Honda, S., & Tsepelev, I. (2013). Linking mantle upwelling with the lithosphere decent and the Japan Sea evolution: A hypothesis. *Scientific Reports*, *3*, 1137. https://doi.org/10.1038/srep01137

Itaki, T. (2016). Transitional changes in microfossil assemblages in the Japan Sea from the late Pliocene to early Pleistocene related to global climatic and local tectonic events. *Progress in Earth and Planetary Science*, *3*(11), 3–11. https://doi.org/10.1186/s40645-016-0087-4

Itaki, T., Sagawa, T., & Kubota, Y. (2018). Data report: Pleistocene radiolarian biostratigraphy, IODP expedition 346 site U1427. In R. Tada, R. W. Murray, C. A. Alvarez Zarikian, & the expedition 346 scientists (Eds.), *Proceedings of the Integrated Ocean drilling Program 346*. Integrated Ocean Drilling Program. https://doi.org/10.2204/iodp.proc.346.202.2018

Itoh, Y., Tsutsumi, H., Yamamoto, H., & Arato, H. (2002). Active right-lateral strike-slip fault zone along the southern margin of the Japan Sea. *Tectonophysics*, *351*, 301–314. https://doi.org/10.1016/s0040-1951(02)00164-6

Katsura, T., & Nagano, M. (1976). Geomorphology and tectonic movement of the sea floor, northwest off Kyushu, Japan. *Journal of Oceanography*, *32*, 139–150. (Japanese with English abstract). https://doi.org/10.1007/bf02107042

Kender, S., Ravelo, A. C., Worne, S., Swann, G. E. A., Leng, M. J., Asahi, H., et al. (2018). Closure of the Bering Strait caused mid-Pleistocene transition cooling. *Nature Communications*, *9*, 5386. https://doi.org/10.1038/s41467-018-07828-0

Kido, Y., Minami, I., Tada, R., Fujine, K., Irino, T., Ikehara, K., et al. (2007). Orbital-scale stratigraphy and high-resolution analysis of biogenic components and deep-water oxygenation conditions in the Japan Sea during the last 640 kyr. *Palaeogeography, Palaeoclimatology, Palaeoecology*, *247*, 32–49. https://doi.org/10.1016/j.palaeo.2006.11.020

Kitaba, I., Harada, M., Hyodo, M., Katoh, S., Sato, H., & Matsushita, M. (2011). MIS 21 and the mid-Pleistocene climate transition: Climate and sea-level variation from a sediment core in Osaka Bay, Japan. *Palaeogeography, Palaeoclimatology, Palaeoecology*, *299*, 227–239. https://doi.org/10.1016/j.palaeo.2010.11.004

Kitaba, I., Hyodo, M., Katoh, S., Dettman, D. L., & Sato, H. (2012). 241 Cyclic vegetation changes during the mid-Pleistocene climate transition around Osaka Bay, southwest Japan. *Japanese Journal of Palynology*, *58*(Special Issue), 110. conference abstract.

Kitamura, A. (1991). Paleoenvironmental transition at 1.2 Ma in the Omma Formation, central Honshu, Japan. *Transactions and Proceedings of the Paleontological Society of Japan*, *162*, 767–780.

Kitamura, A. (2016). Constraints on eustatic sea-level changes during the mid-Pleistocene climate transition: Evidence from the Japanese shallow-marine sediment record. *Quaternary International*, *397*, 417–421. https://doi.org/10.1016/j.quaint.2015.03.004

Kitamura, A., & Kawagoe, T. (2006). Eustatic sea-level change at the mid-Pleistocene climate transition: New evidence from the shallow-marine sediment record of Japan. *Quaternary Science Reviews*, *25*, 323–335. https://doi.org/10.1016/j.quascirev.2005.02.009

Kitamura, A., & Kimoto, K. (2006). History of the inflow of the warm Tsushima Current into the Sea of Japan between 3.5 and 0.8 Ma. *Palaeogeography, Palaeoclimatology, Palaeoecology*, *236*, 355–366. https://doi.org/10.1016/j.palaeo.2005.11.015

Kitamura, A., Takano, O., Takada, H., & Omote, H. (2001). Late Pliocene-early Pleistocene paleoceanographic evolution of the Sea of Japan. *Palaeogeography, Palaeoclimatology, Palaeoecology*, *172*, 81–98. https://doi.org/10.1016/s0031-0182(01)00272-3

Kubota, Y., Kimoto, K., Tada, R., Oda, H., Yokoyama, Y., & Matsuzaki, H. (2010). Variations of East Asian summer monsoon since the last deglaciation based on Mg/Ca and oxygen isotope of planktonic foraminifera in the northern East China Sea. *Paleoceanography*, *25*(4), PA001891. https://doi.org/10.1029/2009pa001891

Lambeck, K., Rouby, H., Pucell, A., Sun, Y., & Sambridge, M. (2014). Sea level and global ice volumes from the Last Glacial Maximum to the Holocene. *Proceedings of the National Academy of Sciences of the United States of America*, *111*(43), 15296–15303. https://doi.org/10.1073/pnas.1411762111

Lear, C. H., Billups, K., Rickaby, R. E. M., Diester-Haass, L., Mawbey, E. M., & Sosdian, S. M. (2016). Breathing more deeply: Deep ocean carbon storage during the mid-Pleistocene climate transition. *Geology*, *44*(12), 1035–1038. https://doi.org/10.1130/g38636.1

Lee, S. H., & Choi, B.-J. (2015). Vertical structure and variation of currents observed in autumn in the Korea Strait. *Ocean Science Journal*, *50*(2), 163–182. https://doi.org/10.1007/s12601-015-0013-5

Lisiecki, L. E., & Raymo, M. E. (2005). A Pliocene-Pleistocene stack of 57 globally distributed benthic $\delta^{18}O$ records. *Paleoceanography*, *20*, PA1003. https://doi.org/10.1029/2004pa001071

Lu, H., Stevens, T., Yi, S., & Sun, X. (2006). An erosional hiatus in Chinese loess sequences revealed by closely spaced optical dating. *Chinese Science Bulletin*, *51*, 2253–2259. https://doi.org/10.1007/s11434-006-2097-x

Maher, B. A., & Thompson, R. (2012). Oxygen isotopes from Chinese caves: Records not of monsoon rainfall but of circulation regime. *Journal of Quaternary Science*, *27*, 615–624. https://doi.org/10.1002/jqs.2553

Martin, P. A., Lea, D. W., Rosenthal, Y., Shackleton, N. J., Sarnthein, M., & Papenfuss, T. (2002). Quaternary deep sea temperature histories derived from benthic foraminiferal Mg/Ca. *Earth and Planetary Science Letters*, *198*, 193–209. https://doi.org/10.1016/s0012-821x(02)00472-7

Martínez-Garcia, A., Rosell-Melé, A., Jaccard, S. L., Geibert, W., Sigman, D. M., & Haug, G. (2011). Southern Ocean dust–climate coupling over the past four million years. *Nature*, *476*, 312–315. https://doi.org/10.1038/nature10310

Matsui, H., Tada, R., & Oba, T. (1998). Low-salinity isolation event in the Japan Sea in response to eustatic sea-level drop during LGM. *The Quaternary Research*, *37*(3), 221–233. (Japanese with English abstract). https://doi.org/10.4116/jaqua.37.221

Meng, X., Liu, L., Wang, X. T., Baslam, W., Chen, J., & Ji, J. (2018). Mineralogical evidence of reduced East Asian summer monsoon rainfall on the Chinese loess plateau during the early Pleistocene interglacials. *Earth and Planetary Science Letters*, *486*, 61–69. https://doi.org/10.1016/j.epsl.2017.12.048

Miller, C., & Dickens, G. (2017). Data report: Reanalysis of interstitial water barium, iron, and sulfur concentrations at Sites U1426 and U1427. In R. Tada, R. W. Murray, C. A. Alvarez Zarikian, & the Expedition 346 scientists (Eds.), *Proceedings of IODP expedition 346* (pp. 7). Integrated Ocean Drilling Program. https://doi.org/10.2204/iodp.proc.346.203.2017

Mudelsee, M., & Schulz, M. (1997). The mid-Pleistocene climate transition: Onset of 100 ka cycle lags ice volume build-up by 280 ka. *Earth and Planetary Science Letters*, *151*, 117–123. https://doi.org/10.1016/s0012-821x(97)00114-3

Nürnberg, D. (1995). Magnesium in tests of Neogloboquadrina Pachyderma sinistral from high northern and southern latitudes. *Journal of Foraminiferal Research*, *25*(4), 350–368.

Oba, T., & Irino, T. (2012). Sea level at the last glacial maximum, constrained by oxygen isotopic curves of planktonic foraminifera in the Japan Sea. *Journal of Quaternary Science*, *27*(9), 941–947. https://doi.org/10.1002/jqs.2585

Oba, T., Kato, M., Kitazato, H., Koizumi, I., Omura, A., Sakai, T., et al. (1991). Paleoenvironmental changes in the Japan Sea during the last 85,000 years. *Paleoceanography*, *6*(4), 499–518. https://doi.org/10.1029/91pa00560

Obreht, I., Zeeden, C., Hambach, U., Veres, D., Marković, S. B., & Lehmkuhl, F. (2019). A critical reevaluation of palaeoclimate proxy records from loess in the Carpathian Basin. *Earth Science Reviews*, *190*, 498–520. https://doi.org/10.1016/j.earscirev.2019.01.020

Okuno, J., Nakada, M., Ishii, M., & Miura, H. (2014). Vertical tectonic crustal movements along the Japanese coastlines inferred from late Quaternary and recent relative sea-level changes. *Quaternary Science Reviews*, *91*, 42–61. https://doi.org/10.1016/j.quascirev.2014.03.010

Pang, X., Bassinot, F., & Sepulcre, S. (2020). Cleaning method impact on the Mg/Ca of three planktonic foraminiferspecies: A downcore study along a depth transect. *Chemical Geology*, *549*, 119690. https://doi.org/10.1016/j.chemgeo.2020.119690

Park, S., & Chu, P. C. (2006). Thermal and haline fronts in the Yellow/East China Seas: Surface and subsurface seasonality comparison. *Journal of Oceanography*, *62*(5), 617–638. https://doi.org/10.1007/s10872-006-0081-3

Pena, L. D., & Goldstein, S. L. (2014). Thermohaline circulation crisis and impacts during the mid-Pleistocene transition. *Science*, *345*, 318–322. https://doi.org/10.1126/science.1249770

Peng, X., Ao, H., Xiao, G., Qiang, X., & Qiang, S. (2020). The early-middle Pleistocene transition of Asian summer monsoon. *Palaeogeography, Palaeoclimatology, Palaeoecology*, *545*, 109636. https://doi.org/10.1016/j.palaeo.2020.109636

Peterson, L. C., & Schimmenti, D. E. (2020). Data report: X-ray fluorescence scanning of Site U1427, Yamato Basin, Expedition 346. In R. Tada, R. W. Murray, C. A. Alvarez Zarikian, & the Expedition 346 scientists (Eds.) In *Proceedings of IODP expedition 346* (pp. 6). Integrated Ocean Drilling Program. https://doi.org/10.2204/iodp.proc.346.206.2020

Pisias, N. G., & Moore, T. C. (1981). The evolution of Pleistocene climate: A data series approach. *Earth and Planetary Science Letters*, *52*, 450–458. https://doi.org/10.1016/0012-821x(81)90197-7

Porter, S. C., & An, Z. (1995). Correlation between climate events in the north Atlantic and China during the last glaciation. *Nature*, *375*, 305–308. https://doi.org/10.1038/375305a0

Raymo, M. E., Kozdon, R., Evans, D., Lisiecki, L., & Ford, H. L. (2018). The accuracy of mid-Pliocene δ^{18}O-based ice volume and sea level reconstructions. *Earth Science Reviews*, *177*, 291–302. https://doi.org/10.1016/j.earscirev.2017.11.022

Raymo, M. E., Oppo, D. W., & Curry, W. (1997). The mid-Pleistocene climate transition: A deep sea carbon isotopic perspective. *Paleoceanography*, *12*(4), 546–559. https://doi.org/10.1029/97pa01019

Roberts, J., Gottschalk, J., Skinner, L. C., Peck, V. L., Kender, S., Elderfield, H., et al. (2016). Evolution of South Atlantic density and chemical stratification across the last deglaciation. *Proceedings of the National Academy of Sciences of the United States of America*, *113*(3), 514–519. https://doi.org/10.1073/pnas.1511252113

Rohling, E. J., Foster, G. L., Grant, K. M., Marino, G., Roberts, A. P., Tamisiea, M. E., et al. (2014). Sea-level and deep-sea-temperature variability over the past 5.3 million years. *Nature*, *508*(7497), 477–482. https://doi.org/10.1038/nature13230

Rosenthal, Y. (2007). Elemental proxies for reconstructing Cenozoic seawater paleotemperatures from calcareous fossils. In C. Hillaire-Marcel, & A. De Vernal (Eds.), *Developments in marine geology* (pp. 765–797). Elsevier. https://doi.org/10.1016/s1572-5480(07)01024-x

Rosenthal, Y., Boyle, E., & Slowey, N. (1997). Temperature control on the incorporation of magnesium, strontium, fluorine, and cadmium into benthic foraminiferal shells from Little Bahama Bank: Prospects for thermocline paleoceanography. *Geochimica et Cosmochimica Acta*, *61*(17), 3633–3643. https://doi.org/10.1016/s0016-7037(97)00181-6

Rosenthal, Y., Perron-Cashman, S., Lear, C. H., Bard, E., Barker, S., Billups, K., et al. (2004). Interlaboratory comparison study of Mg/Ca and Sr/Ca measurements in planktonic foraminifera for paleoceanographic research. *Geochemistry, Geophysics, Geosystems*, *5*(4), GC000650. https://doi.org/10.1029/2003gc000650

Ruddiman, W. F. (2001). Chapter 17: Humans and climate change. In W. F. Ruddiman, & author (Eds.), *Earth's climate – past and future* (pp. 383–404). W.H. Freeman and Company.

Ruddiman, W. F. (2003). Orbital insolation, ice volume, and greenhouse gases. *Quaternary Science Reviews*, *22*, 1597–1629. https://doi.org/10.1016/s0277-3791(03)00087-8

Ruddiman, W. F. (2004). The role of greenhouse gases in orbital-scale climatic changes. *EOS Magazine*, *285*(1), 6–7. https://doi.org/10.1029/2004EO010002

Saavedra-Pellitero, M., Baumann, K.-H., Gallagher, S. J., Sagawa, T., & Tada, R. (2019). Paleoceanographic evolution of the Japan Sea over the last 460 kyr – A coccolithophore perspective. *Marine Micropaleontology*, *152*, 101720. https://doi.org/10.1016/j.marmicro.2019.01.001

Sagawa, T., Ikehara, K., Irino, T., Nakagawa, T., Takahashi, S., Kubota, Y., et al. (2015). *Cruise report of R/V Kairei, KR15-10, precise chronology for the late Pleistocene Japan Sea sediments and its application to paleoceanography off Wakasa Bay* (pp. 58). Japan Agency for Marine-Earth Science and Technology (JAMSTEC).

Sagawa, T., Nagahashi, Y., Satoguchi, Y., Holbourn, A., Itaki, T., Gallagher, S. J., et al. (2018). Integrated tephrostratigraphy and stable isotope stratigraphy in the Japan Sea and East China Sea using IODP Sites U1426, U1427, and U1429, Expedition 346 Asian Monsoon. *Progress in Earth and Planetary Science*, *5*, 18. https://doi.org/10.1186/s40645-018-0168-7

Sexton, P. E., & Wilson, P. A. (2009). Preservation of benthic foraminifera and reliability of deep-sea temperature records: Importance of sedimentation rates, lithology, and the need to examine test wall structure. *Paleoceanography*, *24*, PA2208. https://doi.org/10.1029/2008pa001650

Shackleton, N. J. (2000). The 100,000 year ice age cycle identified and found to lag temperature, carbon dioxide and orbital eccentricity. *Science*, *289*, 1989–1902. https://doi.org/10.1126/science.289.5486.1897

Shackleton, N. J., & Opdyke, N. D. (1976). Oxygen-isotope and paleomagnetic stratigraphy of Pacific core V28-239: Late Pliocene to latest Pleistocene. *Memoirs of the Geological Society of America*, *145*, 449–464. https://doi.org/10.1130/mem145-p449

Skinner, L., Menviel, L., Broadfield, L., Gottschalk, J., & Greaves, M. (2020). Southern Ocean convection amplified past Antarctic warming and atmospheric CO_2 rise during Heinrich Stadial 4. *Communications Earth and Environment*, *1*. https://doi.org/10.1038/s43247-020-00024-3

Son, M., Song, C. W., Kim, M.-C., Cheon, Y., Cho, H., & Sohn, Y. K. (2015). Miocene tectonic evolution of the basins and fault systems, SE Korea: Dextral, simple shear during the East Sea (Sea of Japan) opening. *Journal of the Geological Society*, *172*(5), 664–680. https://doi.org/10.1144/jgs2014-079

Sosdian, S., & Rosenthal, Y. (2009). Deep-sea temperature and ice volume changes across the Pliocene-Pleistocene climate transitions. *Science*, *325*, 306–310. https://doi.org/10.1126/science.1169938

Sosdian, S., Rosenthal, Y., & Toggweiler, J. R. (2018). Deep Atlantic carbonate ion and CaCO3 compensation during the ice ages. *Paleoceanography and Paleoclimatology*, *33*, 546–562. https://doi.org/10.1029/2017pa003312

Stirpe, C. R., Allen, K. A., Sikes, E. L., Zhou, X., Rosenthal, Y., Cruz-Uribe, A. M., et al. (2021). The Mg/Ca proxy for temperature: A Uvigerina core-top study in the southwest Pacific. *Geochemica et Cosmochemica Acta*, *309*, 299–312. https://doi.org/10.1016/j.gca.2021.06.015

Tada, R. (1994). Paleoceanographic evolution of the Japan Sea. *Paleogeography, Paleoclimatology, Paleoecology*, *108* (3–4), 487–508. https://doi.org/10.1016/0031-0182(94)90248-8

Tada, R. (2004). Onset and evolution of millennial-scale variability in the Asian Monsoon and its impact on paleoceanography of the Japan Sea. In P. D., Clift, W., Kuhnt, P., Wang, & D., Hayes (Eds.) *Continent-ocean interactions in the east Asian marginal seas*. (Vol. 149, pp. 283–298). AGU Monograph. https://doi.org/10.1029/149gm15

Tada, R., Irino, T., Ikehara, K., Karasuda, A., Sugisaki, S., Xuan, C., et al. (2018). High-resolution and high-precision correlation of dark and light layers in the Quaternary hemipelagic sediments of the Japan Sea recovered during IODP Expedition 346. *Progress in Earth and Planetary Sciences*, *5*, 19. https://doi.org/10.1186/s40645-018-0167-8

Tada, R., Irino, T., Koizumi, I. (1999). Land-ocean linkages over orbital and millennial timescales recorded in late Quaternary sediments of the Japan Sea. *Plaeoceanography*, *14*(2): 236–247. https://doi.org/10.1029/1998pa900016

Tada, R., Koizumi, I., Cramp, A., & Rahman, A. (1992). Correlation of dark and light layers, and the origin of their cyclicity in the Quaternary sediments from the Japan Sea. In K. A., Pisciotto, J. C., Ingle Jr, M. T., von Breymann, J., Barron, S. C. Clemens, G. R. Dickens, et al. (Eds.), *Proceedings of the Ocean Drilling Program, scientific results. Part (1)*, (Vol. 127/128, pp. 577–601). Ocean Drilling Program. https://doi.org/10.2973/odp.proc.sr.127128-1.160.1992

Tada, R., Murray, R. W., Alvarez Zarikian, C. A., Anderson, W. T., Jr, Bassetti, M.-A., Brace, B. J., et al. (2013) *Proceedings of IODP expedition 346*. Integrated Ocean Drilling Program. https://doi.org/10.2204/iodp.proc.346.2015

Tada, R., Murray, R. W., Alvarez Zarikian, C. A., Anderson, W. T., Jr, Bassetti, M.-A., Brace, B. J., et al. (2015a). Expedition summary. In R. Tada, R. W. Murray, C. A. Alvarez Zarikian, & the Expedition 346 scientists (Eds.) *Proceedings of the Integrated Ocean drilling Program*, (Vol. 346). Integrated Ocean Drilling Program. https://doi.org/10.2204/iodp.proc.346.108.2015

Tada, R., Murray, R. W., Alvarez Zarikian, C. A., Anderson, W. T., Jr, Bassetti, M.-A., Brace, B. J., et al. (2015b). Site U1427 Summary. In R. Tada, R. W. Murray, C. A. Alvarez Zarikian, & the Expedition 346 scientists (Eds.) *Proceedings of the Integrated Ocean drilling Program*, (Vol. 346). Integrated Ocean Drilling Program. https://doi.org/10.2204/iodp.proc.346.108.2015

Tamaki, K., Suyehiro, K., Allan, J., Ingle, J. C., & Pisciotto, K. A. (1992). 83. Tectonic synthesis and implications of Japan Sea ODP drilling. In K. Pisciotto, K. Tamaki, J. Allan, J. M. Alexandrovich, D. A. Barnes, S. Boggs, et al. (Eds.) *Proceedings of the Ocean Drilling Program, scientific results, part 2*, (Vol. 127/128 pp. 1333–1348). Ocean Drilling Program.

Tomczak, M., & Godfrey, J. S. (1994) *Regional oceanography: An introduction*. Pergamon, (pp. 422).

Wang, Y., Cheng, H., Edwards, R. L., Kong, X., Shao, X., Chen, S., et al. (2008). Millennial and orbital-scale changes in the East Asian Monsoon over the past 224,000 years. *Nature*, *451*, 1090–1093. https://doi.org/10.1038/nature06692

Wang, Y. J., Cheng, H., Edwards, R. L., An, Z. S., Wu, J. Y., Shen, C. C., et al. (2001). A high-resolution absolute-dated late Pleistocene monsoon record from Hulu Cave, China. *Science*, *294*, 2345–2348. https://doi.org/10.1126/science.1064618

Watanabe, S., Tada, R., Ikehara, K., Fujine, K., & Kido, Y. (2007). Sediment fabrics, oxygenation history, and circulation modes of Japan Sea during the Late Quaternary. *Palaeogeography, Palaeoclimatology, Palaeoecology*, *247*(1–2), 50–64. https://doi.org/10.1016/j.palaeo.2006.11.021

Yoon, S. (1997). Miocene-Pleistocene volcanism and tectonics in southern Korea and their relationship to the opening of the Japan Sea. *Tectonophysics*, *281*, 53–70. https://doi.org/10.1016/s0040-1951(97)00158-3

Zachos, J. C., Pagani, M., Sloan, L., Thomas, E., & Billups, K. (2001). Trends, rhythms, and aberrations in global climate 65 Ma to present. *Science*, *292*, 686–693. https://doi.org/10.1126/science.1059412

Zhang, W., De Vleeshouwer, D., Shen, J., Zhang, Z., & Zeng, L. (2018). Orbital time scale records of Asian eolian dust from the Sea of Japan since the early Pliocene. *Quaternary Science Reviews*, *187*, 157–167. https://doi.org/10.1016/j.quascirev.2018.03.004

Zhang, W., Jin, F.-F., Stuecker, M. F., Wittenberg, A. T., Timmermann, A., Ren, H.-L., et al. (2016). Unraveling El Niño's impact on the East Asian monsoon and Yangtze River summer flooding. *Geophysical Research Letters*, *43*, 11375–11382. https://doi.org/10.1002/2016GL071190

References From the Supporting Information

Bentov, S., & Erez, J. (2006). Impact of biomineralization processes on the Mg content of foraminiferal shells: A biological perspective. *Geochemistry, Geophysics, Geosystems*, *7*, Q01P08. https://doi.org/10.1029/2005gc001015

Bryan, S. P., & Marchitto, T. M. (2008). Mg/Ca–temperature proxy in benthic foraminifera: New calibrations from the Florida Straits and a hypothesis regarding Mg/Li. *Paleoceanography*, *23*, PA2220. https://doi.org/10.1029/2007PA001553

Casazza, L. R. (2012). *Symbiosis in the fossil record: Eocene nummulites and pleistocene reefs of Egypt. PhD thesis* (pp. 115). University of California.

Collen, J. D., & Burgess, C. J. (1979). Calcite dissolution, overgrowth and recrystallization in the benthic foraminiferal genus Notorotalia. *Jounal of Paleontology*, *53*(6), 1343–1353.

D'Hondt, S., & Arthur, A. (1996). Late Cretaceous oceans and the cool tropic paradox. *Science*, *271*, 1838–1841. https://doi.org/10.1126/science.271.5257.1838

Edgar, K. M., Pälike, H., & Wilson, P. A. (2013). Testing the impact of diagenesis on the $\delta^{18}O$ and $\delta^{13}C$ of benthic foraminiferal calcite from a sediment burial depth transect in the equatorial Pacific. *Paleoceanography*, *28*, 468–480. https://doi.org/10.1002/palo.20045

Emery, W. E., & Tomson, R. E. (2001). *Data analysis methods in physical oceanography* (2nd ed.). Elsevier Science. https://doi.org/10.1016/B978-0-444-50756-3.X5000-X

Flügel, E. (2004). Integrated facies analysis. In E. Flügel, & author (Eds.), *Microfacies of carbonate rocks – analysis, interpretation and application* (pp. 646). Springer. https://doi.org/10.1007/978-3-662-08726-8_13

Fox, L. R., & Wade, B. S. (2013). Systematic taxonomy of early-middle Miocene planktonic foraminifera from the equatorial Pacific Ocean: Integrated ocean drilling program, site U1338. *Journal of Foraminiferal Research*, *43*(4), 374–405. https://doi.org/10.2113/gsjfr.43.4.374

Goyet, C., Healy, R., & Ryan, J. (2000). Global distribution of total inorganic carbon and total alkalinity below the deepest winter mixed layer depths. Carbon Dioxide Information Analysis Center, Oak Ridge National Laboratory, U.S. Department of Energy. 756 ORNL/CDIAC-127, NDP-076. https://doi.org/10.3334/cdiac/otg.ndp076

Isobe, A. (2020). Paleo-ocean destratification triggered by the subduction of the Oyashio water into the Sea of Japan after the Last Glacial Maximum. *Paleoceanography and Paleoclimatology*, *35*, e2019PA003593. https://doi.org/10.1029/2019PA003593

Itaki, T., Ikehara, K., Motoyama, I., & Hasegawa, S. (2004). Abrupt ventilation changes in the Japan Sea over the last 30 ky: Evidence from deep-dwelling radiolarians. *Palaeogeography, Palaeoclimatology, Palaeoecology*, *208*, 263–278. https://doi.org/10.1016/j.palaeo.2004.03.010

Katz, A. (1973). The interaction of magnesium with calcite during crystal growth at 25–90 ºC and one atmosphere. *Geochimica et Cosmochimica Acta*, *37*, 1563–1586. https://doi.org/10.1016/0016-7037(73)90091-4

Lamb, J. L., & Miller, T. H. (1984). *Stratigraphic significance of Uvigerninid foraminifers in the western hemisphere*. Harold Norman Fisk Memorial Papers. No. 66. Exxon Company.

Lear, C. H., Elderfield, H., & Wilson, P. A. (2000). Cenozoic deep-sea temperatures and global ice volumes from Mg/Ca in benthic foraminiferal calcite. *Science*, *287*, 269–272. https://doi.org/10.1126/science.287.5451.269

Lear, C. H., Rosenthal, Y., & Slowey, N. (2002). Benthic foraminiferal Mg/Capaleothermometry: A revised core-top calibration. *Geochemica et Cosmochemica Acta*, *66*(19), 3375–3387. https://doi.org/10.1016/s0016-7037(02)00941-9

Lewis, E., & Wallace, D. (1998). *Program Developed for CO_2 System Calculations. ORNL/CDIAC-105*. Carbon Dioxide Information Analysis Center, Oak Ridge National Laboratory.

Marchitto, T. M., Bryan, S. P., Curry, W. B., & McCorkle, D. C. (2007). Mg/Ca temperature calibration for the benthic foraminifer *Cibicidoides pachyderma*. *Paleoceanography*, *22*, PA1203. https://doi.org/10.1029/2006PA001287

Martin, P. A., & Lea, D. W. (2002). A simple evaluation of cleaning procedures on fossil benthic foraminiferal Mg/Ca. *Geochemistry, Geophysics, Geosystems*, *3*(10), 8401. https://doi.org/10.1029/2001gc000280

Mawbey, E. M., Hendry, K. R., Greaves, M. J., Hillenbrand, C.-D., Kuhn, G., Spencer-Jones, C. L., et al. (2020). Mg/Ca-Temperature calibration of polar benthic foraminifera species for reconstruction of bottom water temperatures on the Antarctic shelf. *Geochemica et Cosmochemica Acta*, *283*, 54–66. https://doi.org/10.1016/j.gca.2020.05.027

Nomaki, H., Heinz, P., Nakatsuka, T., Shimanaga, M., & Kitazato, H. (2005). Species-specific ingestion of organic carbon by deep-sea benthic foraminifera and meiobenthos: In situ tracer experiments. *Limnology and Oceanography*, *50*(1), 134–146. https://doi.org/10.4319/lo.2005.50.1.0134

Ohga, T., & Kitazato, H. (1997). Seasonal changes in bathyal foraminiferal populations in response to the flux of organic matter (Sagami Bay, Japan). *Terra Nova*, *9*(1), 33–37. https://doi.org/10.1046/j.1365-3121.1997.d01-6.x

Oomori, T., Kaneshima, H., Maezato, Y., & Kitano, Y. (1987). Distribution coefficient of Mg^{2+} ions between calcite and solution at 10–50°C. *Marine Chemistry*, *20*(4), 327–336. https://doi.org/10.1016/0304-4203(87)90066-1

Pearson, P. N., & Burgess, C. (2008). Foraminifer shell preservation and diagenesis: Comparison of high latitude Eocene sites. In W. E. N. Austin, & R. H. James (Eds.), *Biogeochemical controls on palaeoceanographic proxies* (Vol. 303, pp. 59–72). Geological Society of London, Special Publications. https://doi.org/10.1144/SP303.5

Pearson, P. N., Ditchfield, P. W., Singano, J., Harcourt-Brown, K. G., Nicholas, C. J., Olsson, R. K., et al. (2001). Warm tropical sea surface temperatures in the Late Cretaceous and Eocene epochs. *Nature*, *413*, 481–487. https://doi.org/10.1038/35097000

Pearson, P. N., Evans, S. L., & Evans, J. (2015). Effect of diagenetic recrystallization on the strength of planktonic foraminifer tests under compression. *Journal of Micropaleontology*, *34*(1), 59–64. https://doi.org/10.1144/jmpaleo2013-032

Rathburn, A. E., & De Deckker, P. (1997). Magnesium and strontium compositions of Recent benthic foraminifera from the Coral Sea, Australia and Prydz Bay, Antarctica. *Marine Micropaleontology*, *32*(3–4), 231–248. https://doi.org/10.1016/s0377-8398(97)00028-5

Rosenthal, Y., & Boyle, E. (1993). Factors controlling the fluoride content of planktonic foraminifers: An evaluation of its paleoceanographic applicability. *Geochimica et Cosmochimica Acta*, *57*, 335–346. https://doi.org/10.1016/0016-7037(93)90435-y

Sexton, P. E., Wilson, P. A., & Pearson, P. N. (2006). Microstructural and geochemical perspectives on planktic foraminiferal preservation: "glassy" versus "frosty". *Geochemistry, Geophysics, Geosysystems*, *7*(12), GC001291. https://doi.org/10.1029/2006gc001291

Shackleton, N. J. (1974). Attainment of isotopic equilibrium between ocean water and the benthonic foraminifera genus *Uvigerina*: Isotopic changes in the ocean during the Last Glacial. Colloques Internationaux de C.N.R.S. *Les methods quantitatives d'etude des variations du climat au cours du Pléistocène, no. 219*, (pp. 203–209).

Tachikawa, K., & Elderfield, H. (2002). Microhabitat effects on Cd/Ca and $\delta^{13}C$ of benthic foraminifera. *Earth and Planetary Science Letters*, *202*(3–4), 607–624. https://doi.org/10.1016/s0012-821x(02)00796-3

Talley, L. D., Lobanov, V., Ponomarev, V., Salyuk, A., Tishchenko, P., Zhabin, I., et al. (2003). Deep convection and brine rejection in the Japan Sea. *Geophysical Research Letters*, *30*(4), 1159. https://doi.org/10.1029/2002GL016451

Voigt, J., Hathorne, E. C., Frank, M., & Holburn, A. (2016). Minimal influence of recrystallization on middle Miocene benthic foraminiferal stable isotope stratigraphy in the eastern equatorial Pacific. *Paleoceanography*, *31*, 98–114. https://doi.org/10.1002/2015pa002822

Wilson, P. A., Norris, R. D., & Cooper, M. J. (2002). Testing the Cretaceous greenhouse hypothesis using glassy foraminiferal calcite from the core of the Turonian tropics on Demerara Rise. *Geology*, *30*, 607–610. https://doi.org/10.1130/0091-7613(2002)030<0607:ttcghu>2.0.co;2

Wilson, P. A., & Opdyke, B. N. (1996). Equatorial sea-surface temperatures for the Maastrichtian revealed through remarkable preservation of metastable carbonate. *Geology*, *24*, 555–558. https://doi.org/10.1130/0091-7613(1996)024<0555:esstft>2.3.co;2

Yu, J., & Elderfield, H. (2008). Mg/Ca in the benthic foraminifera *Cibicidoides wuellerstorfi* and *Cibicidoides mundulus*: Temperature versus carbonate ion saturation. *Earth and Planetary Science Letters*, *276*, 129–139. https://doi.org/10.1016/j.epsl.2008.09.015